Institute of High Frequency Technology

RWTH AACHEN UNIVERSITY

Master Thesis

Evaluation of the Electromagnetic Characteristics of a Rectangular Antenna Test Chamber

Tania del Cerro Sánchez
29-04-2015

Supervisors:

Prof. Dr.-Ing. Dirk Heberling
M. Sc. Hammam Shakhtour

Ich erkläre hiermit, dass ich diese Arbeit selbständig verfaßt, noch nicht anderweitig für andere Prüfungszwecke vorgelegt, keine anderen als die angegebenen Quellen und Hilfsmittel -- bis auf die offizielle Betreuung durch das Institut für Hochfrequenztechnik -- benutzt sowie wörtliche und sinngemäße Zitate als solche gekennzeichnet habe. Weiterihn erkläre ich mein Einverständnis, dass die RWTH Aachen diese Prüfungsleistung den Studenten und Mitarbeitern der RWTH Aachen zur Einsicht überlassen, sowie als Ganzes oder in Auszügen veröffentlichen darf.

Scope of work

When measurements in anechoic chambers are carried out, the recorded values present effects which are related to the chamber performance. In order to quantify these effects a figure of merit for the performance of the anechoic chamber is needed. That is why, in this thesis, the well-known free-space Voltage Standing Wave Ratio (VSWR) technique is applied to characterize a small Antenna Test Chamber (ATC).

Summary

After characterizing the ATC with the well-known free space VSWR technique, we can conclude that this chamber presents good reflectivity results despite its small size. As it was expected, the chamber provides better reflectivity values when the operating frequency is increasing. Being these values better than -30, -32.5 and -45 dB at 4, 10 and 26 GHz, respectively. The errors that the measurements present for a C, X and K band horn antennas at these frequencies, in the main lobe are 0.044, 0.0053 and 0.0019 dB, respectively. As it was expected, the error is smaller when the frequency is increasing. With regarding to the errors that are produced in the side lobe are 1.27, 0.18 and 0.034 dB.

A software tool was developed in order to reproduce the measurements when free space VSWR technique is carried out.

Table of contents

1. Introduction

The aim of this thesis is to characterize an anechoic chamber whose size is relatively small. Anechoic chambers try to create a free space environment. However, this condition is not possible to achieve due mainly to the chambers walls. Some rays that impinge on the walls are reflected into the quiet zone. There are more effects that could introduce error in the measurement zone such as, scattering or interference. These rays introduce ripple in the measurements. Hence, we need to determine the error introduced in the measurement due to the chamber walls. A parameter that is related with the chamber performance is the reflectivity.

After this introduction, the characteristics of the ATC, such as, its size, absorbers type, quiet zone and operational frequency range are explained. The manufacturer of this chamber is Comtest Engineering [1]. The chamber has a rectangular shape and the walls are covered with absorbers. Figure 1 shows a schematic of the chamber with the outer dimensions.

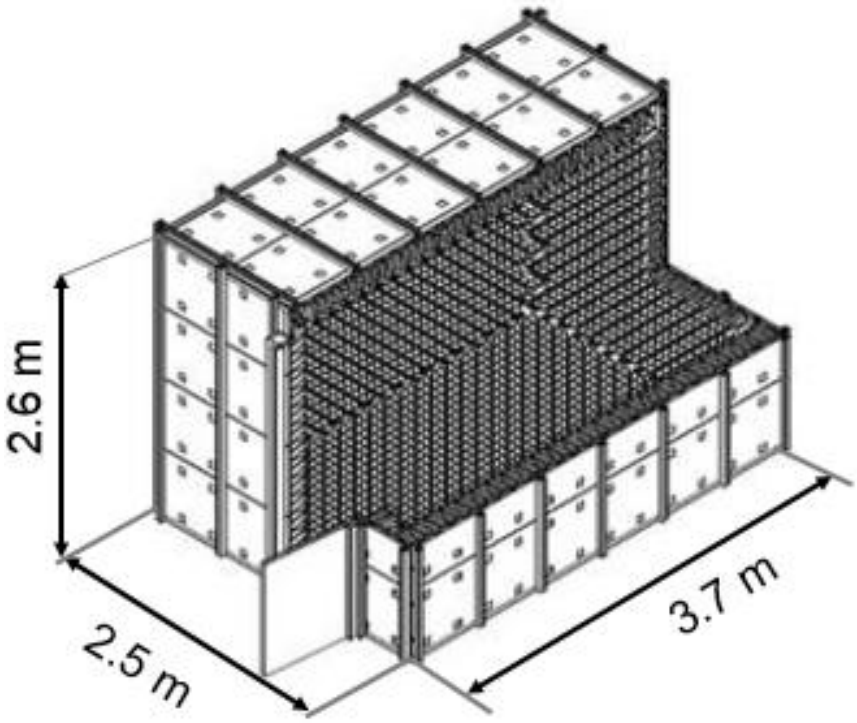

Figure 1 - Rectangular anechoic chamber. Outside view.

It is important to determine the quiet zone of the chamber. Since the chamber is rectangular, the quiet zone shape is circular and its diameter is approximately one third of the chamber width [2]. Hence, in our case the quiet zone diameter is 800 mm, see Figure 2.

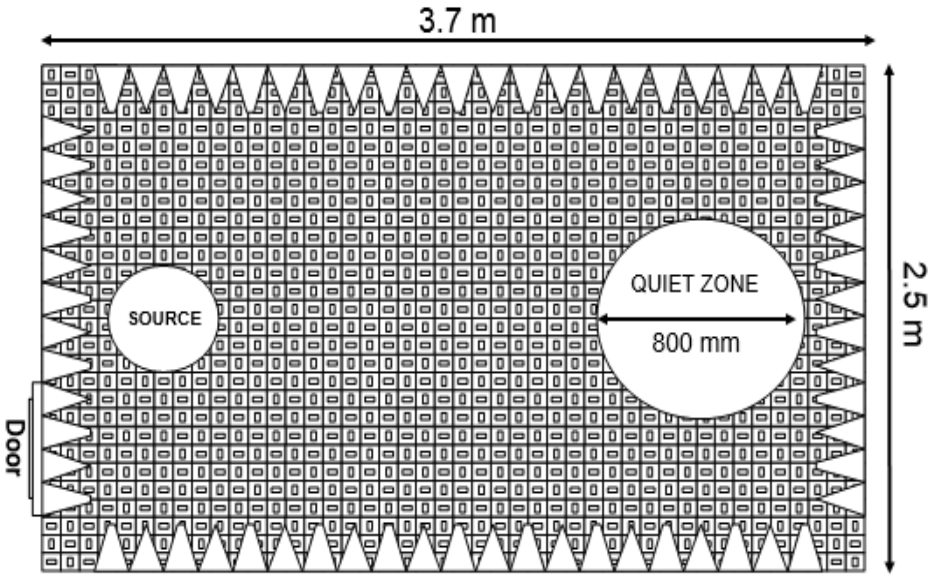

Figure 2 - Rectangular anechoic chamber. Top view.

The chamber uses MT25 pyramidal absorbers. This absorber type is 25 cm height. This is shown in Figure 3.

Figure 3 - MT25 absorbers [3].

This absorber type is designed for Antenna Pattern Measurement, Antenna Test Range, Radar Cross Section and free space testing in anechoic chambers applications [4] [5] [6] .

According to manufacturer, the MT microwave absorbers have high performance and are broadband. They work from 70MHz to 110 GHz. The manufacturer provides graphs (Figure 4 and 5) that show the return loss of MT absorbers at normal incidence for different frequencies.

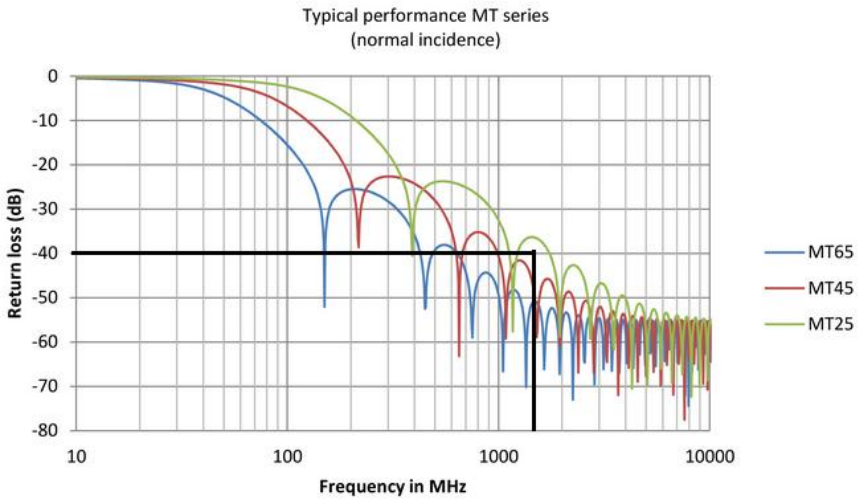

Figure 4 - Return loss MT absorbers performance at normal incidence from 10 MHz to 10 GHz [1].

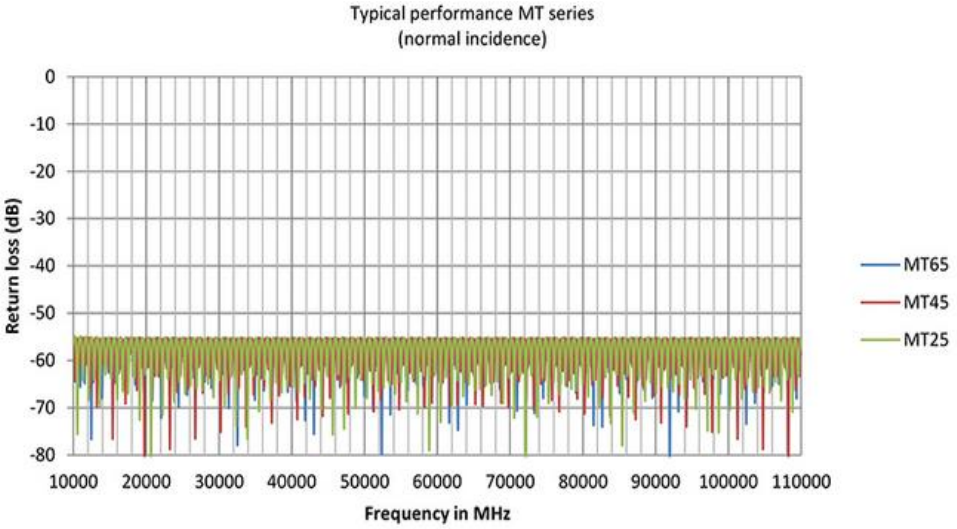

Figure 5- Return loss MT absorbers performance at normal incidence from 10 to 110 GHz [1].

However, for this project we also needed the reflectivity values at different incidence angles. These measurements were taken with the NRL arch system of the Institute.

The operational frequency range of the chamber is the span of frequencies where the chamber can be used. This range is determined by the chamber characteristics and the antennas that are being used. The lowest frequency of the chamber is determined by the worst reflectivity value that we can consider. One common value for this chamber type is 40 dB, as it is explained in [2]. Looking at Figure 4, we can see that in our case the lowest frequency is 1.3 GHz. With regarding to the upper frequency and for far field measurements, we have to take into account that the far field criterion needs to be satisfied. Consequently, depending on the antenna dimension and the chamber size, we obtain the maximum frequency that can be used. However, this value could be limited by the chamber specifications.

The chamber is equipped with a walkway to make the access into the chamber easier. The walkway is made of reinforced glass fibre epoxy grid. It is also equipped with white panels. See Figure 6. The aim of these panels is to create a better illumination inside of the chamber. At the same time, the panels help to protect the RF absorbers. The effects of these accessories are studied in [7].

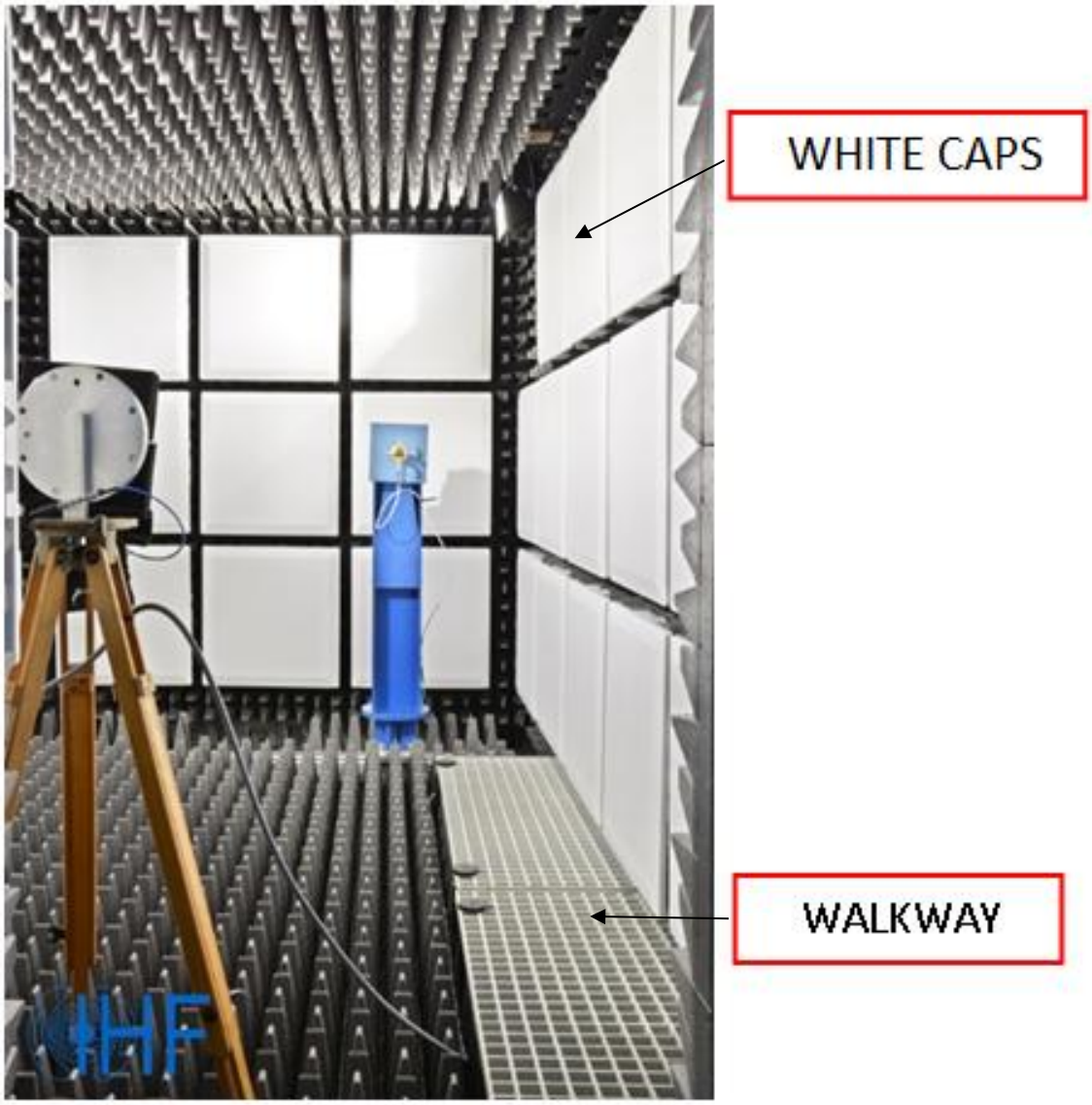

Figure 6 – Picture of the chamber inside.

2. Chamber characterization techniques

There are several existing techniques to characterize anechoic chambers. The most common techniques are explained in this section.

2.1 RCS

This technique tries to find out the chamber reflectivity by calculating the RCS of the chamber with the aid of a reference object and applying time domain technique. Equation [2-1] and [2-2] are used to calculate the reflectivity value. It is required that the far field condition is complied, when a chamber wall is being characterized.

$$RCSchamber = \sigma = \pi R^2 Re^2 \qquad [2\text{-}1]$$

$$RCSchamber = RCSref * \left(\frac{Emp}{Ref}\right)^2 * \left(\frac{D}{R}\right)^4 \quad [m^2] \qquad [2\text{-}2]$$

Where,

R: distance between the antennas and wall.

D: distance between the antennas and the reference object.

Re: wall reflectivity.

RCSchamber: Radar Cross Section of the chamber

RCSref: Radar Cross Section of a reference object.

Emp: received signal when the chamber is empty.

Ref: received signal when a reference object is inside of the chamber.

In [8] a procedure is explained which can be summarized as follows:

1. Transmit and receive antenna are situated close to the front wall. The distance between the antennas and the wall is R, as shown in Figure 8.

2. The first measurement is the empty chamber. The reflection of the back wall is measured. This represents *Emp* in equation [2-2].

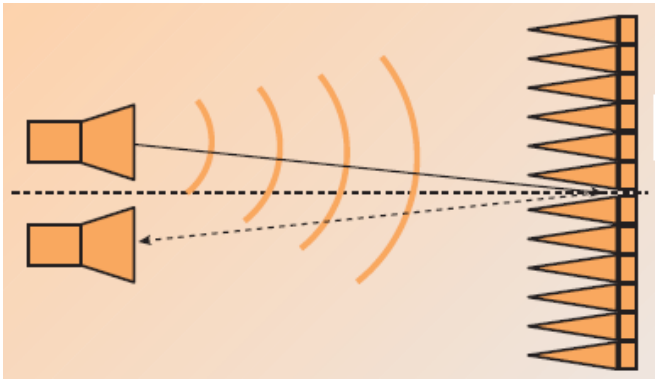

Figure 7 - RCS measurement empty chamber [8].

3. Now a RCS target is introduced in the middle of the quiet zone. The distance between the antennas and this point is D, as shown in Figure 8. The reference object can be a metallic flat plate or a sphere. This will be *Ref* given in equation [2-2].

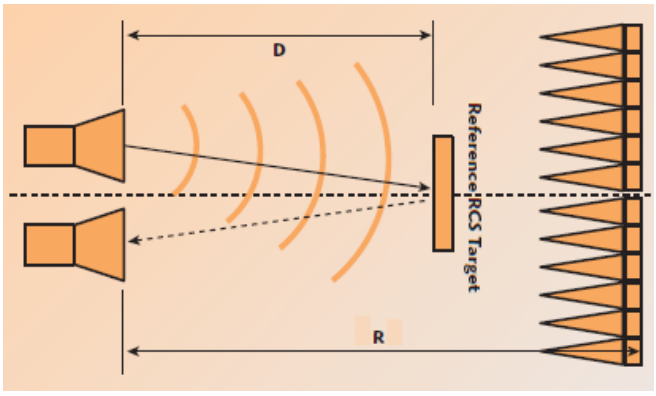

Figure 8- RCS measurement with a reference object [8].

4. Finally, we have all the necessary data to compute the RCS of the chamber, equation [2-2]. Then, replacing this value and the distance between the antennas and the wall in [2-1], we obtain the reflectivity level of the back wall.

   The same procedure is used to characterize the rest of the chamber walls.

2.2 Antenna Pattern Comparison

Antenna pattern comparison uses the pattern variations, at different locations of the quiet zone to compute the reflectivity level of the chamber. The procedure consists of placing the probe antenna in the center of the quiet zone. The pattern is recorded by rotating the antenna with a small angle step. Then we repeat the same procedure at different positions of the quiet zone. All the recorded patterns are normalized with respect to the maximum value and superimposed. The levels of maximum difference between patterns are selected. See Figure 9.b, where transmit and receive antenna situation is shown in Figure 9.a.

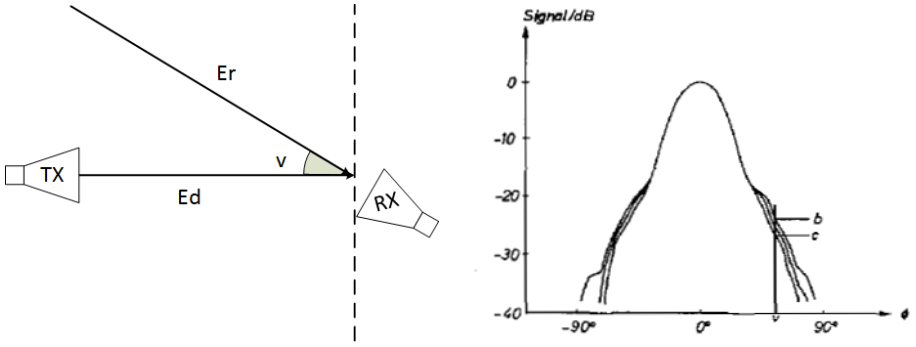

Figure 9- (9.a) Measurement scenario. (9.b) Antenna pattern comparison measurement [9].

Then, with the aid of the equations [2-3] and [2-4] we can know the direct and reflected level of the field. These equations take the maximum and minimum recorded values and the real amplitude of the pattern at the angle where the reflection arrives. By replacing the obtained values in the equation [2-5], the ratio between the reflected and direct rays is known and this relation provide an indication of the chamber performance [9].

$$b = 20log\frac{Ed*10^{\frac{a}{20}}+Er}{Ed} \quad [2\text{-}3]$$

$$c = 20log\frac{Ed*10^{\frac{a}{20}}-Er}{Ed} \quad [2\text{-}4]$$

$$R = 20log\frac{Er}{Ed} \quad [2\text{-}5]$$

Where,

Ed: direct electric field.

Er: reflected electric field.

a: pattern level at v angle.

b, c: maximum and minimum recorded values at v angle.

R: ratio between reflected and direct signal.

2.3 Free- space VSWR

Free-space VSWR (Voltage Standing Wave Ratio) is the technique which has been used to characterize the chamber. The procedure, requirements and limitation of this technique are explained in this section.

2.3.1 Introduction

In anechoic chambers reflections are produced mainly due to the chamber walls. These reflections cause constructive and destructive interferences in the measurements. Due to these interferences the shape of the measurements show ripple. An example of the interaction between two waves is shown in Figure 10.

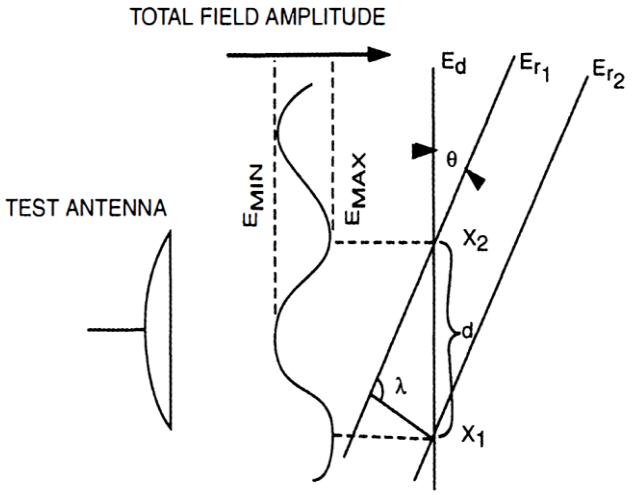

Figure 10- Hypothetical situation of interference due to one reflected wave [2].

Where,

$$Emax = Ed + Er \quad [2\text{-}6]$$

$$Emin = Ed - Er \quad [2\text{-}7]$$

With the aid of the equation [2-8], we can know the ripple level of the measurement.

$$\sigma = \frac{Emax}{Emiin} = 20\log\left(\frac{Ed+Er}{Ed-Er}\right) = 20\log\left(\frac{1+\Gamma}{1-\Gamma}\right) \quad [2\text{-}8]$$

$$\Gamma = \frac{Er}{Ed} \quad [2\text{-}9]$$

Free-space VSWR technique tries to detect all these standing waves in the quiet zone of the chamber. This method tries to find out the worst case of the reflectivity value. The worst case is associated with the maximum ripple of the measurement.

2.3.2 Procedure

The quiet zone is tested with a probe antenna with the aid of a scanning system. The interaction of the direct and reflected rays are recorded. From this data, it is possible to extract the level of the ripples, which are related to the reflectivity level of the chamber, equation [2-10].

The reflectivity value is always referred to boresight. That is why, when the antenna is turned with a certain angle we have to take into account an offset value, in order to compute properly the reflectivity. This term shows the depression level from the main lobe when the receive antenna is rotated with a certain angle.

$$R = 20\log\left(\frac{10^{\frac{\sigma}{20}}-1}{10^{\frac{\sigma}{20}}+1}\right) - offset \qquad [2\text{-}10]$$

A graph exists (Figure 11) that leads also to compute the reflectivity level when the ripple and the depression level is known. As an example, if we have a 0.2 dB ripple that is detected with a depression level of -25dB. Using this graph, one finds out that the reflectivity value in this case is -65 dB.

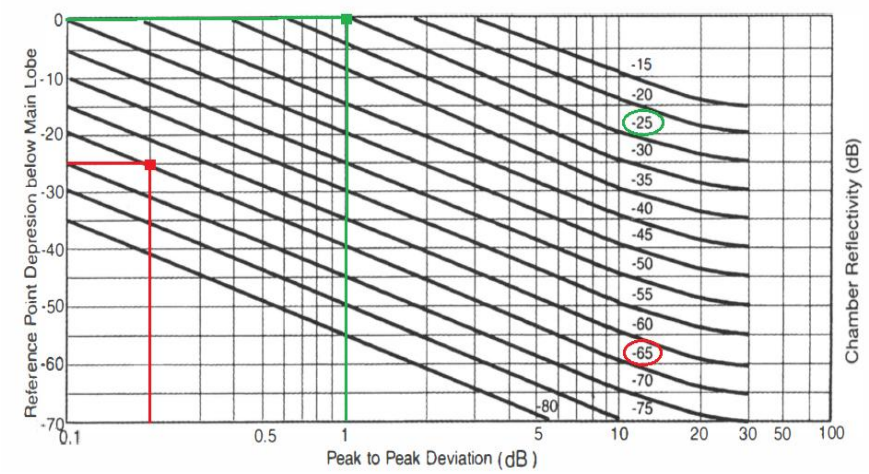

Figure 11 - Graph reflectivity values for different depression levels [2].

At boresight one needs to have the receive and transmit antennas aligned. That is why before starting to develop the technique, it is necessary to carry out an alignment procedure. This has been accomplished using a laser system. If there is a misalignment or tilting between antennas the direct ray not pointing exactly to the maximum of the pattern at boresight.

An important parameter is the scan step which the quiet zone is tested with. If the step is too big, we cannot detect some of the reflections. In contrast, if the step is very small, we can detect the reflections very accurately, but the procedure could be too much time consuming. In ideal case that only one reflection is taking place in the measurement scenario, a suitable step to test the quiet zone is $\lambda/2$ for the highest operating frequency. So that, we can detect the maximum and minimum of the standing waves for the whole operational frequency range. However, this is not the real situation due to there are more reflection involved in the measurement area, so a smaller step is required.

Two scanning schemes are required. Transversal where the scanning takes place on a plane normal to the boresight. The second scheme is the longitudinal and here the scanning takes place on a plane parallel to boresight. After each scan the receiving antenna must be rotated to a new angular position. The angular range that is covered in this thesis is -90° to 90° with a step of 15° .Figure 12 and Figure 13 illustrate these scanning procedures.

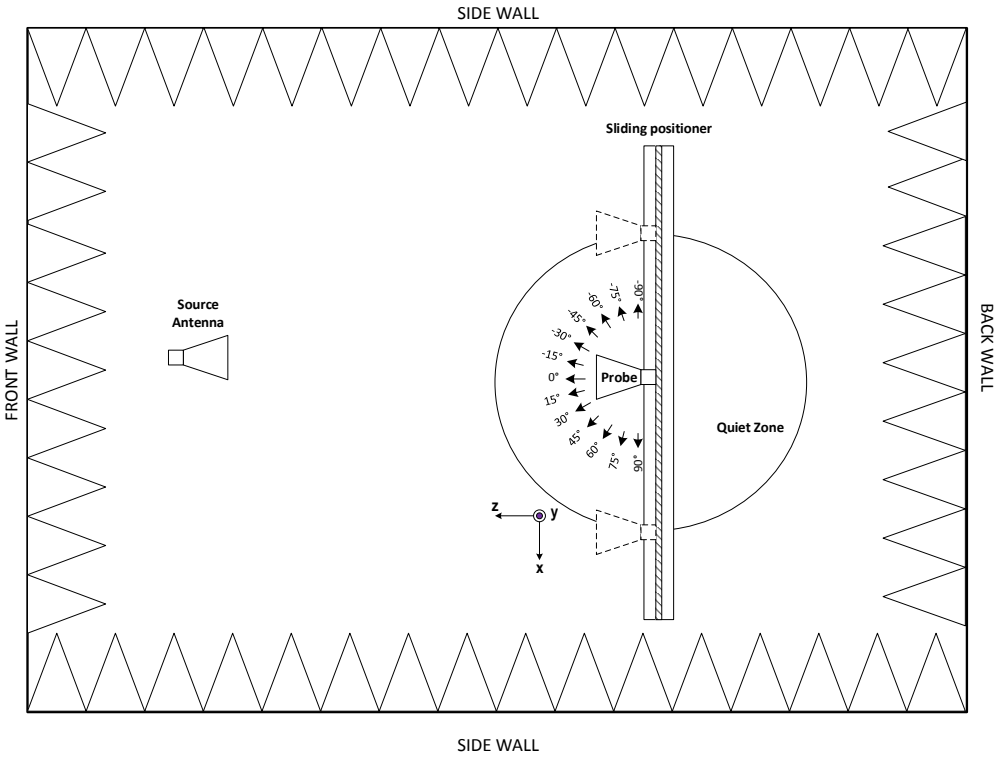

Figure 12- Transversal scan free space VSWR.

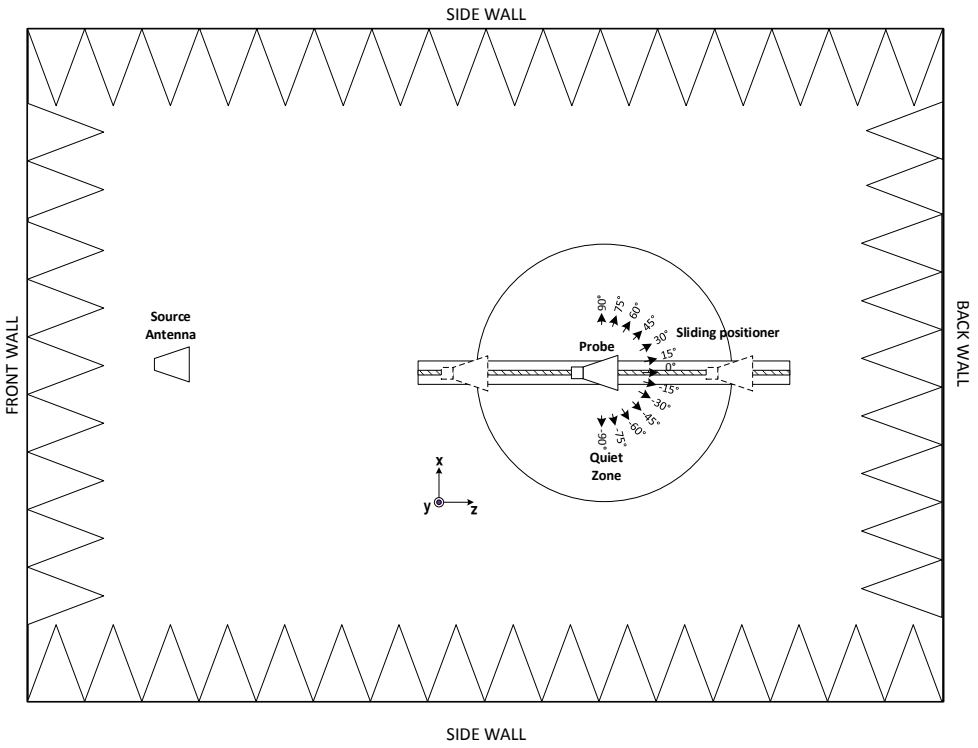

Figure 13- Longitudinal scan free space VSWR.

The procedure of the method is explained below:

1. System Alignment.
2. Do a boresight scan. This is the reference scan needed to compute the offset value in equation [2-10]
3. Do the scan for the rest of the angular range.
4. Calculate the offset value.
5. Compute the reflectivity level using equation [2-10].
6. Do the same procedure for the longitudinal scheme.

When the procedure is carried out, a bigger scan radius than quiet zone one is selected, in order to be able to process correctly the data. Figure 14 shows an example of possible results obtained with this method (Transversal scanning in this case), where the scan radius selected was 0.5 meters. We obtain an offset value of 0.26 dB when receive antenna is +15 degrees rotated.

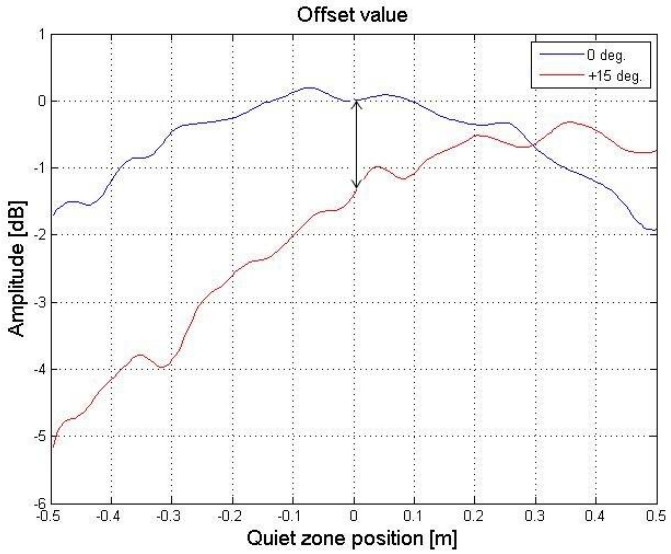

Figure 14- Offset level value.

2.3.3 Antenna requirement

It is advisable to use high gain antenna as a probe, in order to detect as much as possible the standing waves test zone. The level of energy that reaches to the test region is a function of the source antenna pattern. Depending on the amplitude, which source antenna illuminates the side walls, the obtained reflectivity values of the free-space VSWR technique could differ. Obtaining worse reflectivity results if the antenna less directive. A suitable antenna to develop this technique has to have a side lobe of 20dB of depression below the main lobe, which produces a smaller error than ± 1 dB for reflectivity values better than 40 dB [2]. We can calculate this error with the aid of equation [2-11] for the main lobe and [2-12] for the side lobe [10].

$$error = \frac{Ed\sqrt{G(0)} \pm Er\sqrt{G(\theta)}}{Ed\sqrt{G(0)}} \qquad [2\text{-}11]$$

$$error = \frac{Ed\sqrt{G(\theta)} \pm Er\sqrt{G(0)}}{Ed\sqrt{G(\theta)}} \qquad [2\text{-}12]$$

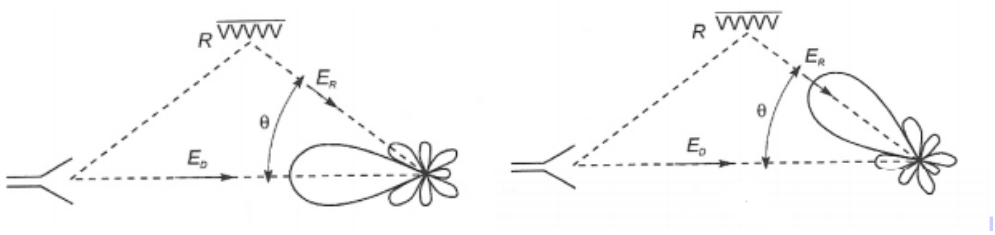

Figure 15– (15.a) Transmit and receive antenna situation eq. 2-11.
(15.b) Transmit and receive antenna situation eq. 2-12 [10].

Another factor that restricts the antenna characteristics is the maximum tapered amplitude that the measurements present in the quiet zone of the chamber. This fact restricts the minimum beamwidth of the antenna. A desirable design in a rectangular chamber is to have less than 0.5 dB amplitude tapered in the quiet zone [2]. However, this value is quite strict and difficult to achieve if we want to comply the previous criterion explained.

It is also important to keep in mind the operational frequency range of the chamber as well as the chamber size. Since this is a far-field technique, this fact restricts the maximum antenna dimension that can be used. Adequate types of antennas are horn or ridge antennas for frequencies above 1 GHz and below 1 GHz LPA (log-periodic array) antennas [2].

2.3.4 Limitation of the technique

This technique shows a limitation, since the quiet zone is scanned at discrete angles, it can happen that some reflections could be missed due to the angle step. A smaller angle step can be used in order to avoid this situation, but the procedure will be too much time consuming. When a high reflectivity value is recorded at certain angle, one option that we can take in order detect if there are more standing waves that could be missed, we can repeat the measurement with a smaller angle step around this angle value [9].

3 Analysis tools

This chapter is divided into two sections, the first one, details the required hardware to develop free-space VSWR. The second one presents a useful tool to analyze the measurements, when this technique is being carried out.

3.1 Hardware

- Two directive antennas and its support system.
- Transmit and receive antenna positioners.
- Two microwave cables.
- Sliding system.
- Controller
- VNA (Vector Network Analyzer).
- Laptop.

Taking into account the antenna requirements to develop the technique, chamber characteristics and the available measurement equipment in the Institute, we selected the antennas for the case under study. Due to chamber characteristic we decided to characterize the chamber in the C, X and K bands. Horn antennas that work at these frequency ranges where selected.

These antennas present a SLL (side lobe level) lower than 20 dB in the whole frequency range. It was as well checked that the size requirement to comply Far-Field criterion is achieved. Table 1 shows the minimum distance between antennas at the highest frequency for each antenna type. Thus, as we can see in this table, transmit and receive antenna has to be separated at least 1.2 meters.

FREQUENCY (GHz)	λ (m)	Diagonal (cm)	R_{MIN} (m)
6	0.05	9	0.324
12	0.025	7.9	0.5
26	0.012	8.5	1.2

Table 1 - Minimum distance required.

These antenna types are supported by a metallic plate, see Figure 16. These supports caused strong reflections. Therefore flat absorbers have been used to cover these plates i.e. put behind the antennas to reduce these reflections.

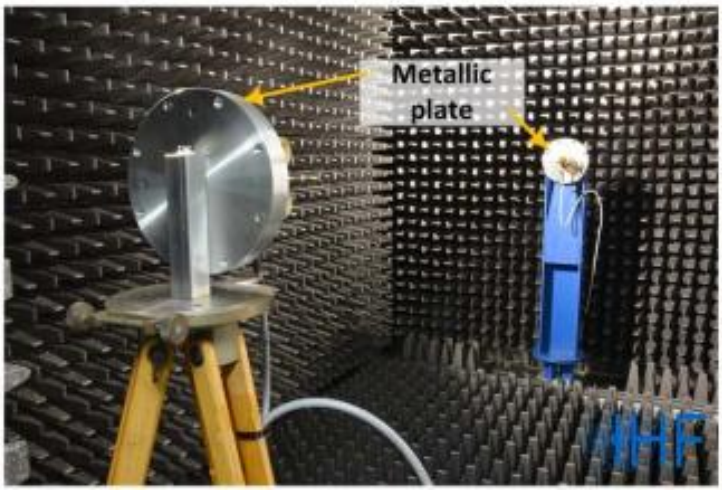

Figure 16 - Antenna supporting system.

Figure 17 shows a simple diagram of the setup that has been used.

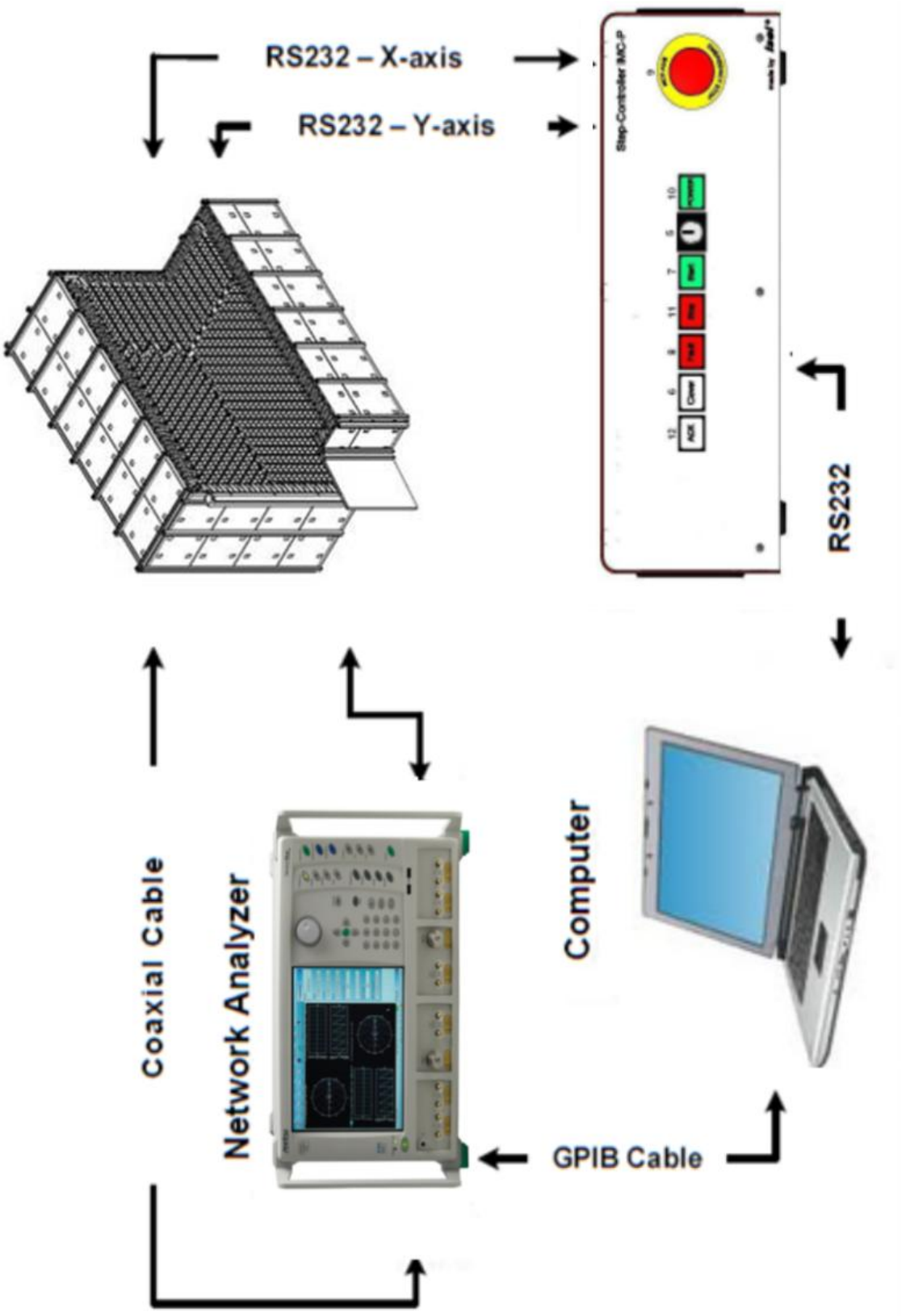

Figure 17 - Measurement equipment.

3.2 Software

A software that implements free-space VSWR technique has been developed. The theoretical base of this software is explained in the next section.

3.2.1 Ray-tracing

When an antenna is in presence of a PEC or PMC surface a fictitious source is generated, this source is called antenna image. It is located at the same height as the real antenna, but at the opposite side of the surface. The direction of the antenna current depends on how the antenna is oriented and the surface type, as shown in Figure 18.

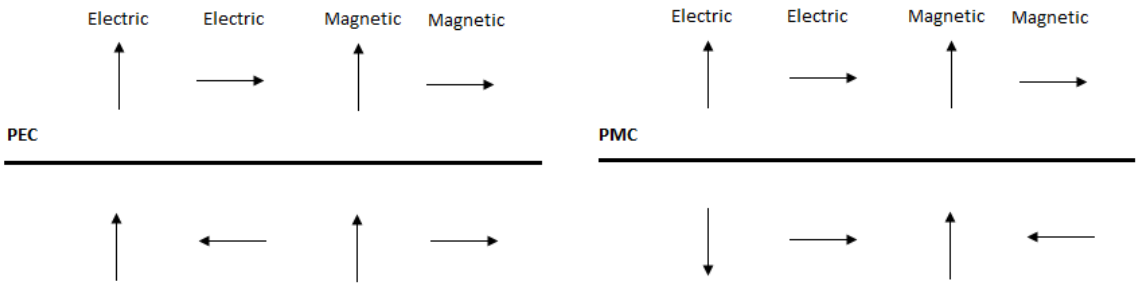

Figure 17- Image theory. Field directions.

If the surface presents a reflection coefficient different than the unity, the ray that comes from the image antenna has to be attenuated by this factor. Based on this phenomenon, ray-tracing is carried out to determine where the reflected rays are impinging.

Ray-tracing tries to simulate the path of the source antenna rays in an indoor or outdoor range. It depends on chamber geometry, antenna locations and image theory. Figure 19 shows the reflections that in a rectangular chamber are produced, where the distance between antennas is Dt and the distance between receive antenna and back wall Dq.

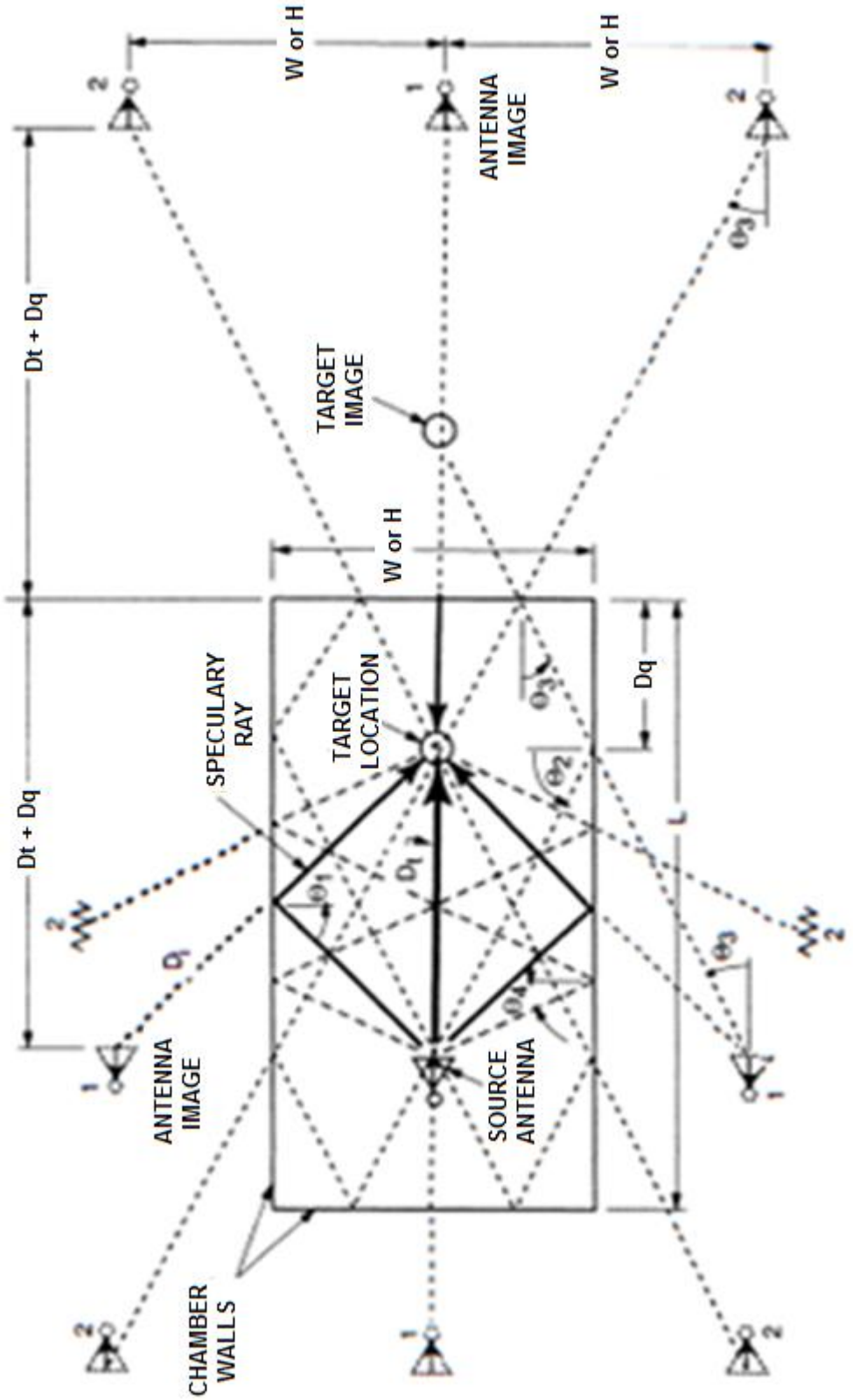

Figure 19- Ray tracing technique in a rectangular anechoic chamber [2].

In Figure 19, the direct ray and the specular rays are drawn as heavy solid lines. These are the specular reflections from side walls, ceiling and ground. As we can see in the picture, these reflections are produced in the middle of the distance between transmit and receive antenna. That is why, usually, in rectangular anechoic chambers, these places are covered by bigger absorbers to reduce these reflection as much as possible [10]. Reflections in the back and front wall are produced by the illumination of the transmit antenna with the main beam and back lobe, respectively.

Each of the reflected rays can be analyzed as energy that comes from an image of the source antenna (image source antennas are drawn in the picture). The images associated with a single-bounce reflection are simply the antenna's mirror image in the wall that the ray hits. The images related with the two-bounce reflections are produced by the antenna side lobes. The procedure can be applied on reflections that present more bounces. The energy of these image sources is attenuated by the reflection coefficient of the surface, in this case, this value is the reflectivity of the absorbers.

In order to compute the total incident field, due to the direct and all types of reflected rays, we calculate the Friis equation for each ray. Equation [3-1] computes the receive power due to the direct ray and equation [3-2] its phase. For reflected rays, equations [3-3] and [3-4] are for the amplitude and phase, respectively [11] .

$$Prx = Ptx + Gtx(\theta tx) + 20\log\left(\frac{\lambda}{4\pi R}\right) + Grx(\theta rx) + \text{PLF} \quad [3\text{-}1]$$

$$\phi_{direct} = kR \quad [3\text{-}2]$$

$$Prx = Ptx + Gtx(\theta tx) + 20\log\left(\frac{\lambda}{4\pi d1}\right) + 10log\Gamma 1 + 20\log\left(\frac{\lambda}{4\pi d2}\right) + 10log\Gamma 2 + \cdots + Grx(\theta rx) + PLF \quad [3\text{-}3]$$

$$\phi_{reflected} = k(d1 + d2) \quad [3\text{-}4]$$

Where,

Ptx: transmitted power
R: distance between transmit and receive antenna
d1, d2: different reflected ray paths
Gtx(Θtx): transmit antenna gain at the transmission angle.
Grx(Θrx): receive antenna gain at the received angle.
Γ1, Γ2: reflection coefficients.
PLF: losses factor.
k: is $2\pi/\lambda$

Depending on the polarization selected, the critical walls will be the ceiling and ground or side walls. To explain this fact we have to know boundary conditions of the electric field in a PEC, equation [3-5]. This fact implies that, only electric perpendicular field to the surface will be different to 0 [12]. Thus, when the

polarization is vertical the main reflected rays will be from the ceiling and ground and for horizontal the side walls. However, the material which the chamber is made of is not a PEC. Therefore, even when the polarization is vertical or horizontal we can receive part of the energy that impinges in parallels surfaces.

$$E\ x\ n = 0 \qquad [3\text{-}5]$$

However, ray tracing cannot be applied in all the scenarios. If the absorbers size is comparable to the wavelength, the reflected ray is not specular. In this case, scattering is the predominant effect when the rays impinges into the absorbers [13] [14].

3.2.2 Antennas pattern

In order to compute the amplitude of the reflected rays correctly, information of the antenna pattern is required. Therefore, the antennas that have been selected to implement free-space VSWR have to be simulated in CST in order to obtain their radiations patterns at different operational frequencies. These results need to be imported in Matlab to apply ray-tracing.

The antennas model and their patterns are shown below, in order to provide a visual example about the CST simulations, figures 20, 21 and 22 are given.

- C Band (4-6 GHz)

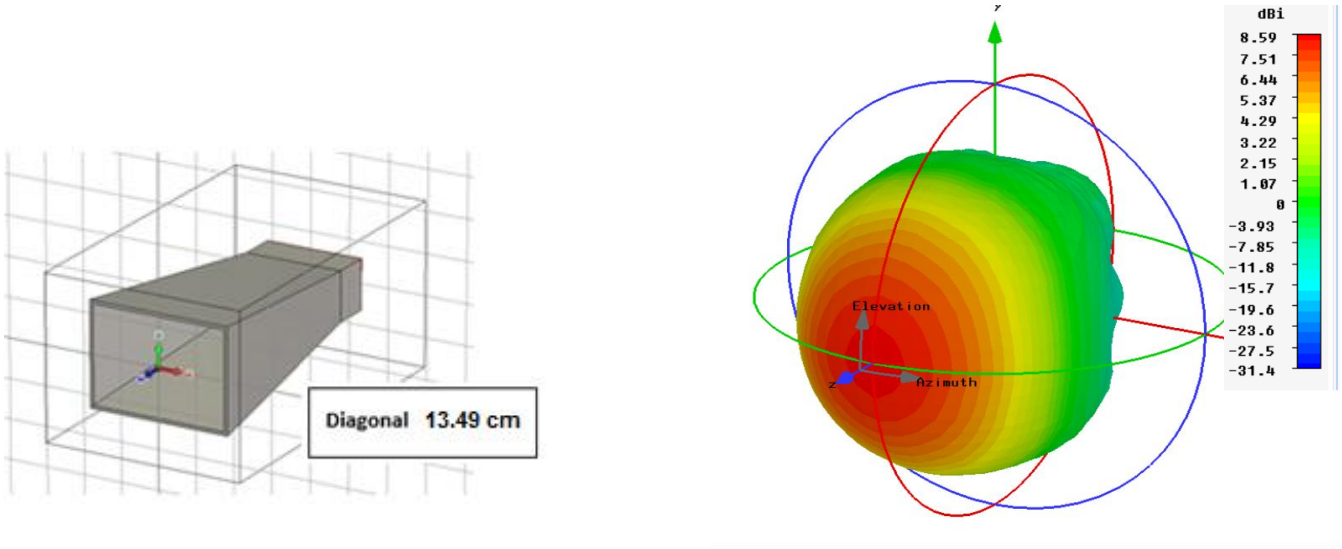

Figure 18- (20.a) C band horn structure.
(20.b) Radiation pattern C band horn antenna at 5GHz.

- X Band (8-12 GHz)

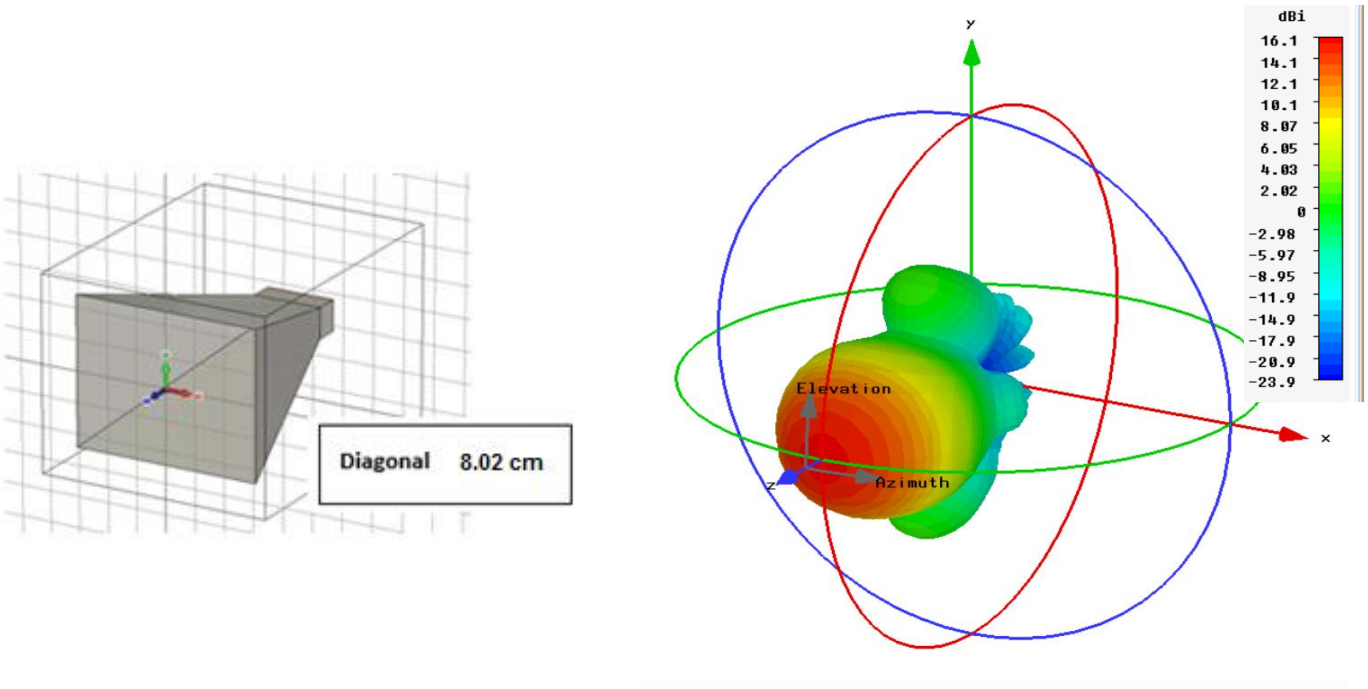

Figure 19– (21.a) X band horn structure.
(21.b) Radiation pattern X band horn antenna at 11.5 GHz.

- K Band (17.5-26 GHz)

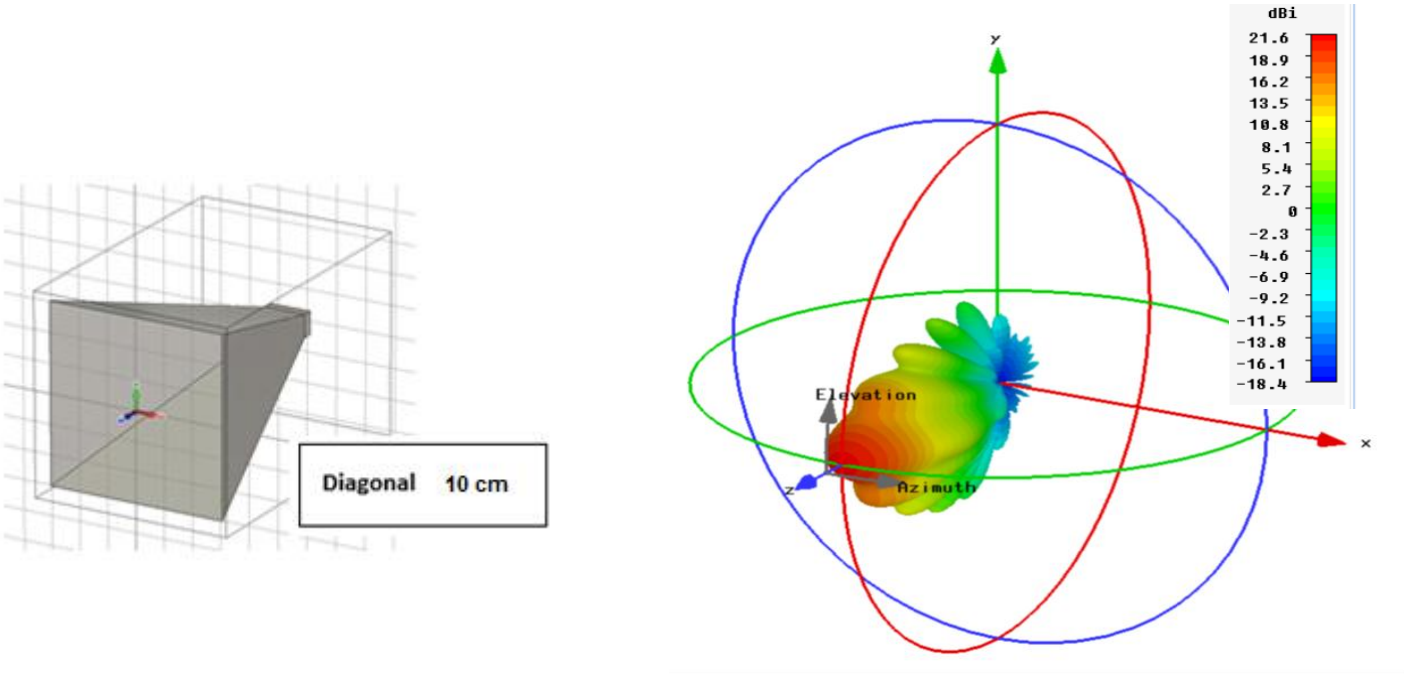

Figure 20- (22.a) K band horn structure.
(22.b) Radiation pattern K band horn antenna at 26 GHz.

3.2.3 Absorbers characterization

The different reflectivity values of the absorber at different incidence angles in the operational frequency range are required. In the manufacturer specification, only the reflectivity values at normal incidence are provided. In order to get such information, the absorbers need to be characterized. That is why the NRL arch system of the institute was used. See Figure 23.

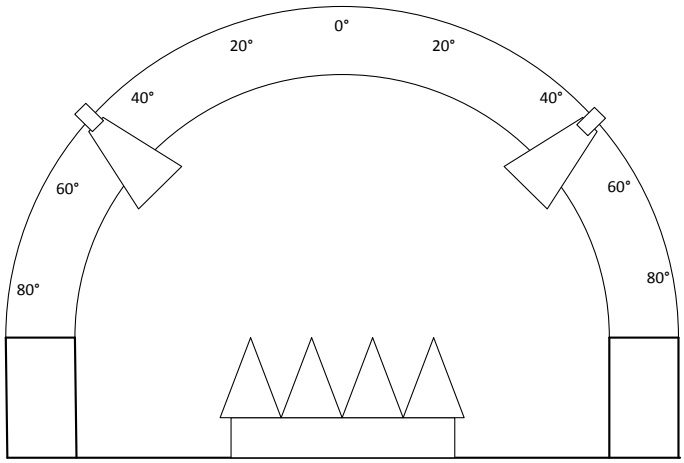

Figure 21- NRL arch system.

We have to bear in mind that this technique can present error in the measurement. Some of them are explained below:

- If transmit and receive antenna are situated close to each other there is a mutual coupling between them.
- Undesired reflections, due to the arch and measurement equipment.
- Due to the small distance between antennas, far field condition is not complied. So that, we are taking the measurements with a spherical wave. Consequently, we have a taper amplitude and an error phase in our results.

Figures 24 and 25 show the results of applying this technique for C and X band, respectively:

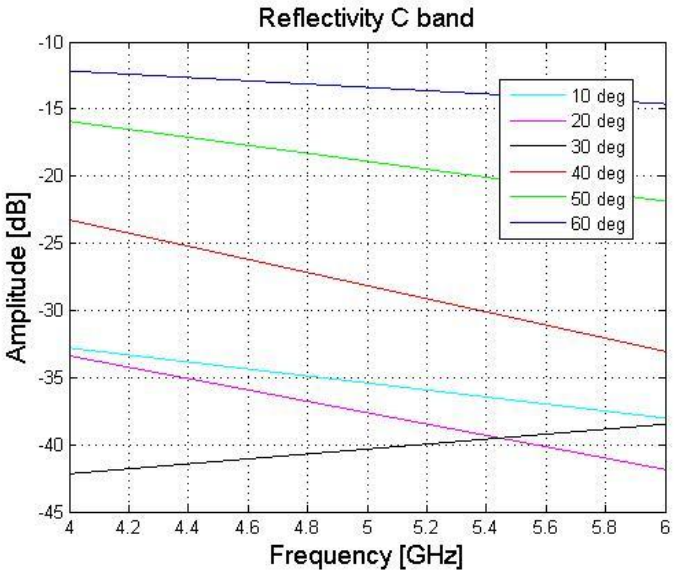

Figure 22 - C band reflectivity results.

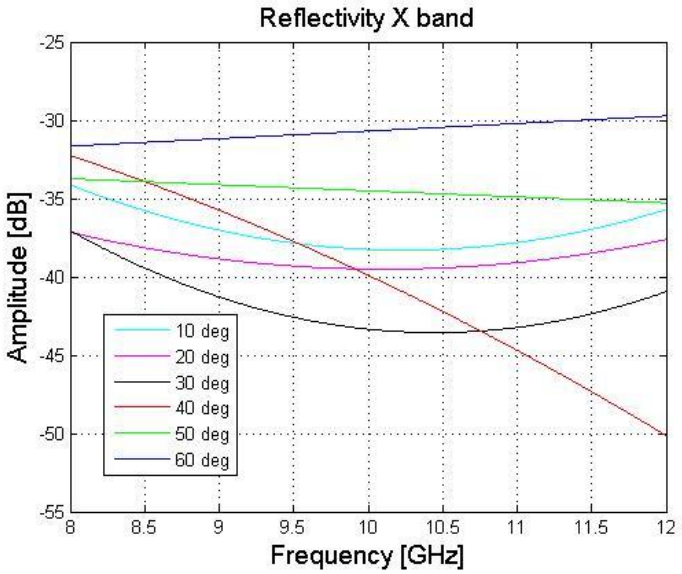

Figure 23 - X band reflectivity results.

It must be mentioned that the C band measurements are erroneous due to the fact that the bandwidth available was not enough to resolve the mutual coupling between the antennas in the time domain. Moreover it was not possible to include absorbing material to minimize the mutual coupling effect without any extra modifications of the setup.

3.2.4 Implementation

The software implements the different movements of the receive antenna when free space VSWR is carried out in the ATC. Then, ray tracing is applied in each situation. This software needs a lot of input parameters. That is why a GUI was implemented, Figure 26.

The following gives an overview of the different inputs needed by the GUI:

- **View:** there are two available modes implemented in this software. *Scan line*, leads to record the data with a scan step at the different positions of the quiet zone, on a plane parallel or perpendicular to boresight. *Sweep boresight*, provides the data at boresight situation in the frequency range of each antenna.

- **Antenna size:** diagonal of the antenna is needed in order to check if Far-Field criterion is complied, as well as, when reflections rays impinge into the receive antenna or not.

- **Chamber size:** here all the characteristics of the chamber are introduced. *Width, height* and *length* are the outside dimension of the chamber. Then, the absorber height is also introduced. *Front wall* and *back wall* are the distances from the antennas to the absorbers of the front and back wall, respectively. *Width shift* and *height shift* express the difference between distances from the antennas to each of the side walls. *Min.distance* represents the minimum distance that we want to have between antennas when longitudinal scan is carried out.

- **Misalignment:** where we can introduce the imbalance between antennas in the alignment process.

- **Frequency:** where the operational frequency of the scan is defined. Depending on this parameter the antenna pattern is selected. *Max. frequency,* defines the maximum frequency that is going to be used in the characterization procedure.

- **Scan characteristics**: where the scan type and polarization are selected. *Turn* represents the angular position of the receive antenna. *Step* defines the scan step which the ATC is tested with. We can introduce this value or we can use the default step which is lambda divided by two at the highest frequency. Finally, *QZ radius* determines the radius of the quiet zone. It can be determined in the text field or we can use the default value which is the chamber width divided by six.

- **View results:** we can select the type ray that we want to visualize, as well as, the type of the wave front. It is also possible to take into account free space losses.

- **Post processing:** to process the result of the scan we can visualize the fitting of signal or calculating its envelope.

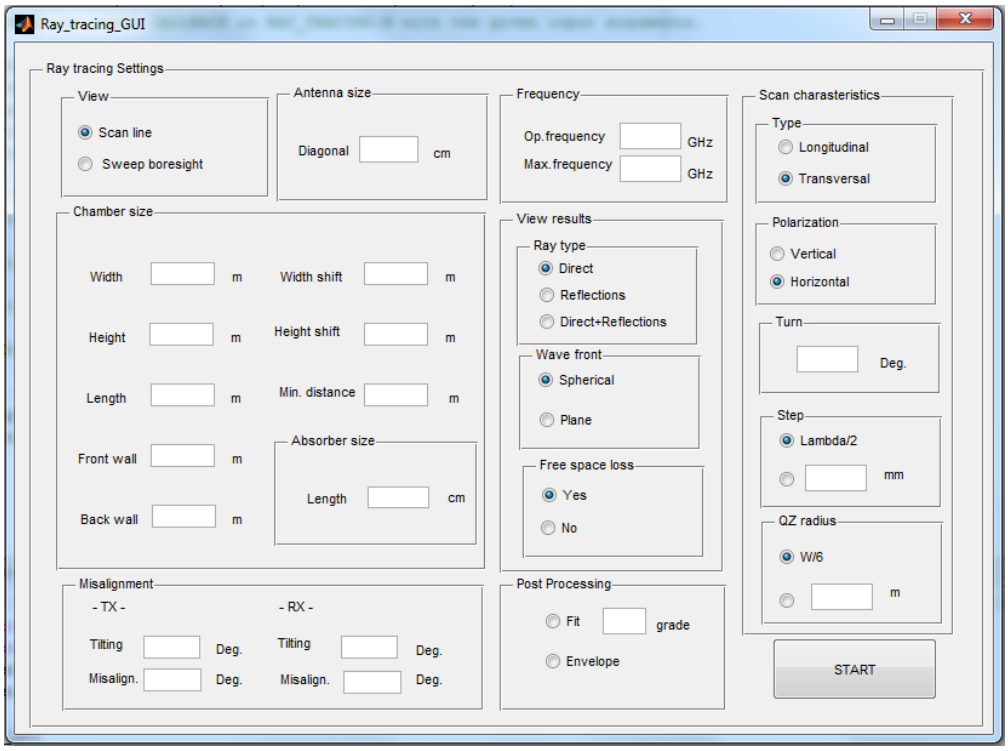

Figure 24 - Ray tracing interface

Figures 27 and 28 provide a visual example of a chamber with these parameters. In the figure, the angle direction and its required sign are also specified.

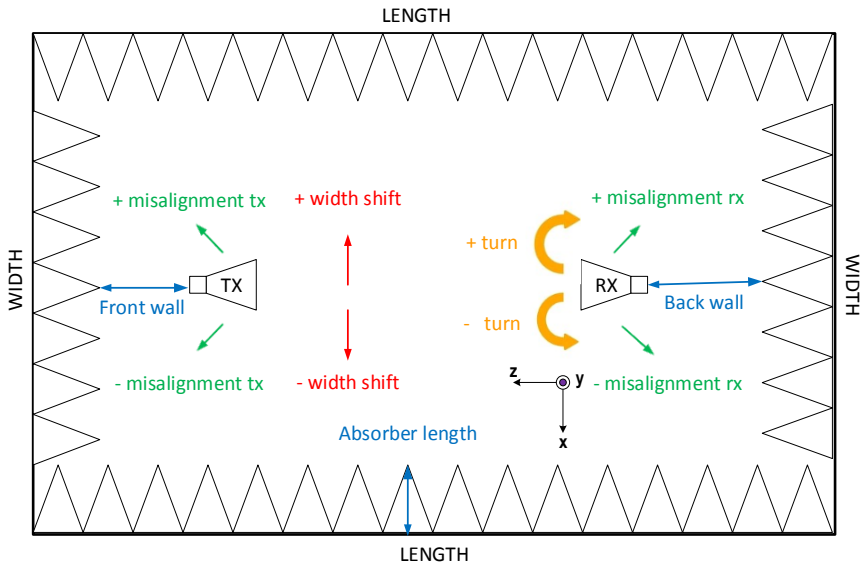

Figure 25 - Chamber view side walls. GUI parameters.

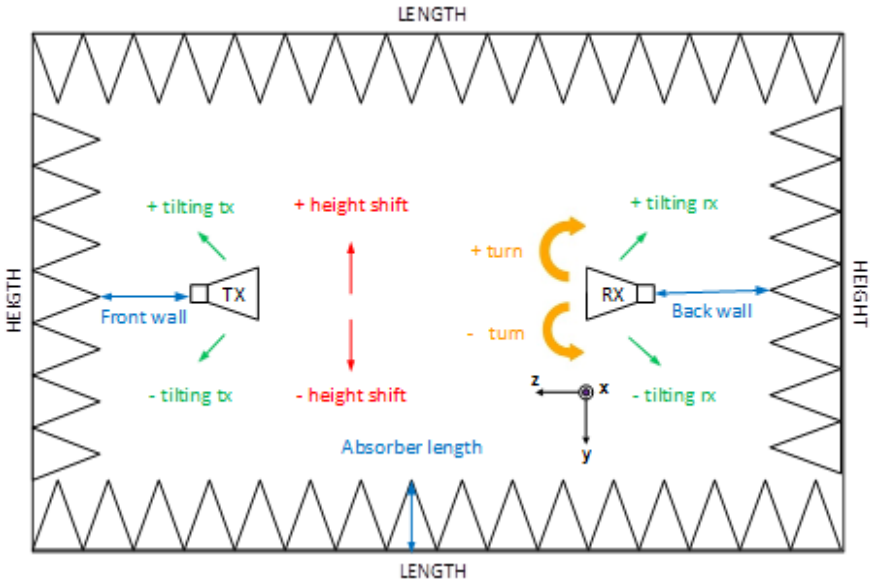

Figure 26 - Chamber view ceiling and ground. GUI parameters.

As it was said in section 3.2.1, when the polarization is vertical, the main reflections come from ceiling and ground. In case of the horizontal polarization, from the side walls. That is why in the software, depending on the polarization, side walls, ceiling or ground effects are neglected. If the scan type is longitudinal, the reflections from the back wall are also important, since the receive antenna is pointed to it. We also take into account the reflections that are produced by side lobes and back lobe of the transmit antenna. Then, in order to compute Friis equation for each ray, the next information is required: angle which is transmitted and received the ray, the gain of the pattern at these angles, reflectivity value at the incidence angle (in case of the reflected rays) and the distance of the path. Here, it is explained how and which reflections are calculated for each situation depending on the scan type and polarization.

- Transversal scan & horizontal polarization.

If transmit and receive antenna are situated in the middle of the chamber width, there is no misalignment between them and the receive antenna is situated in the middle of the quiet zone, reflection rays are symmetric for the side walls. Transmit and receive angle of a specular reflection are the same. When a shift between walls is presented, as in Figure 29, the arrival angle of the reflected rays will be different for both side walls.

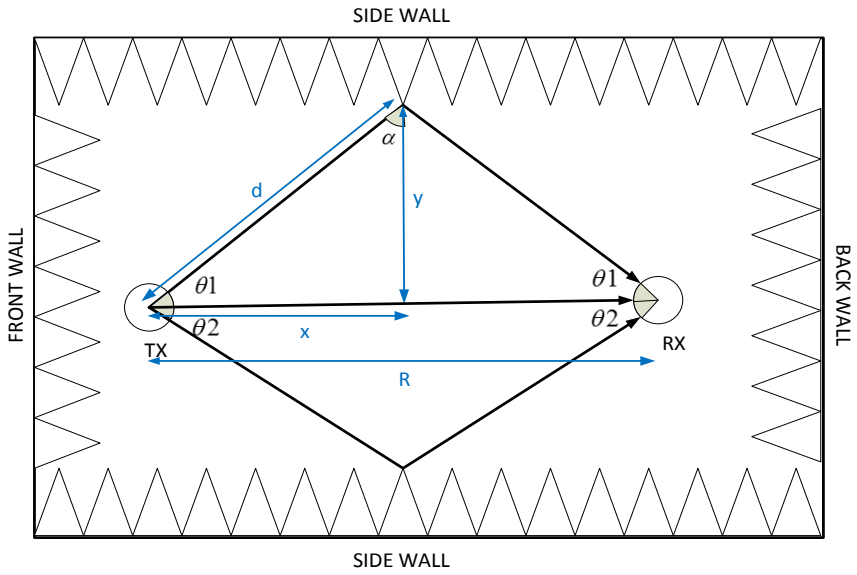

Figure 27 - Specular reflection side walls.

Using the equation [3-6] and replacing the different distances to the side wall, this angle is calculated.

$$\theta = atan\left(\frac{y}{x}\right) \qquad [3\text{-}6]$$

We also need to compute the angle which the reflected ray impinges into the absorber, equation [3-7]. Depending on the incidence angle and frequency, we select the reflectivity value using the recorded data of the previous section.

$$\alpha = 90 - \theta; \qquad [3\text{-}7]$$

The distance of the reflected ray is calculated with the equation [3-8].

$$d = 2 * \sqrt{x^2 + y^2} \qquad [3\text{-}8]$$

With regarding to the direct ray, when the antennas are at boresight and if there is no misalignment, the received angle is 0 degrees and the distance is R.

Next step consists of taking the gain value of each ray at the incidence angle. The E-plane of the pattern is selected. In this case, with the reference angles that we are using, the required plane is azimuth equal to zero. Figure 30 shows an example of the E-plane of the X band antenna at 11.5 GHz.

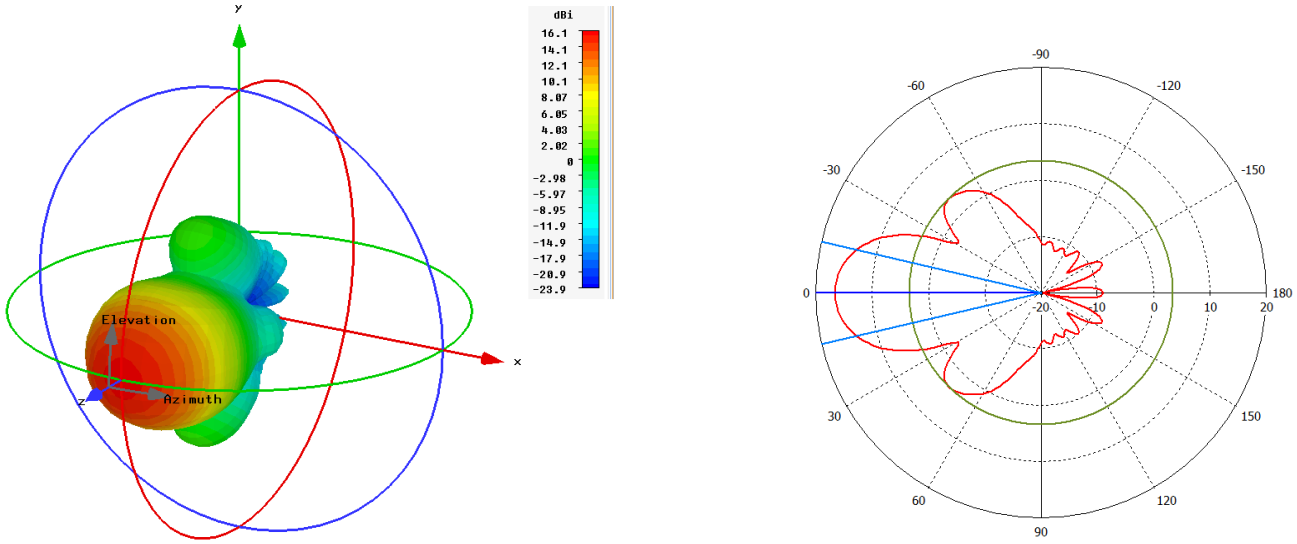

Figure 28 - (30.a) X-Band 3D antenna pattern at 11.5 GHz.
(30.b) E-plane at 11.5 GHz.

By replacing all the information calculated in the equation [3-1] and [3-2], for the direct ray; [3-3] and [3-4], for the reflected, we obtain the phase and power amplitude of the field, at boresight situation. This is the reference value to compute the offset. We continue with the procedure in order to compute the specular reflected rays when a transversal scan is carried out (equation [3-9], [3-10] and [3-11]). Figure 31 shows the incidence angles of the reflected ray in an arbitrary position of this scan.

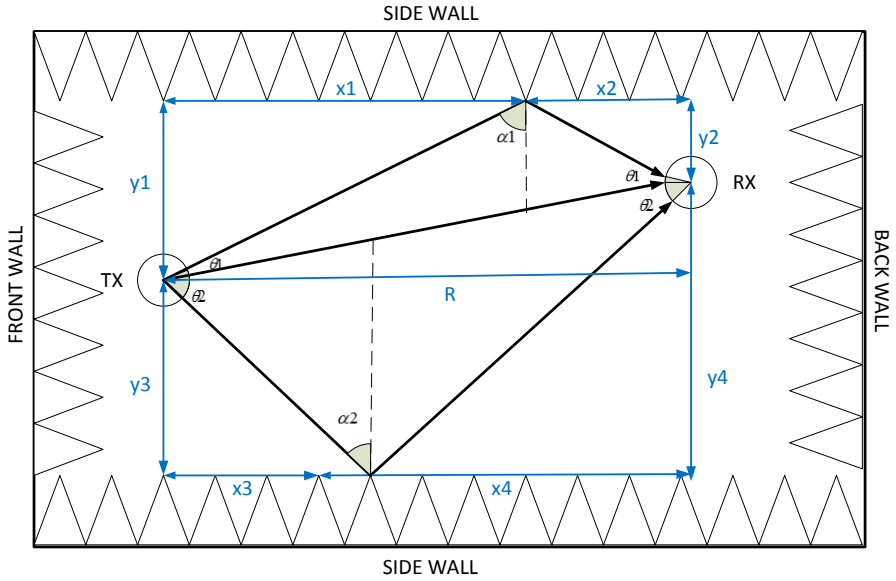

Figure 29 –Transversal scan. Direct and reflection.

$$x1 = y1 * \frac{R}{y1+y2} \quad [3\text{-}9]$$

$$x2 = R - x1 \quad [3\text{-}10]$$

$$\theta 1 = 90 - atan\left(\frac{x1}{y1}\right) \quad [3\text{-}11]$$

Figure 32 shows the direct ray at this situation. With the equation [3-12], the incidence angle is calculated.

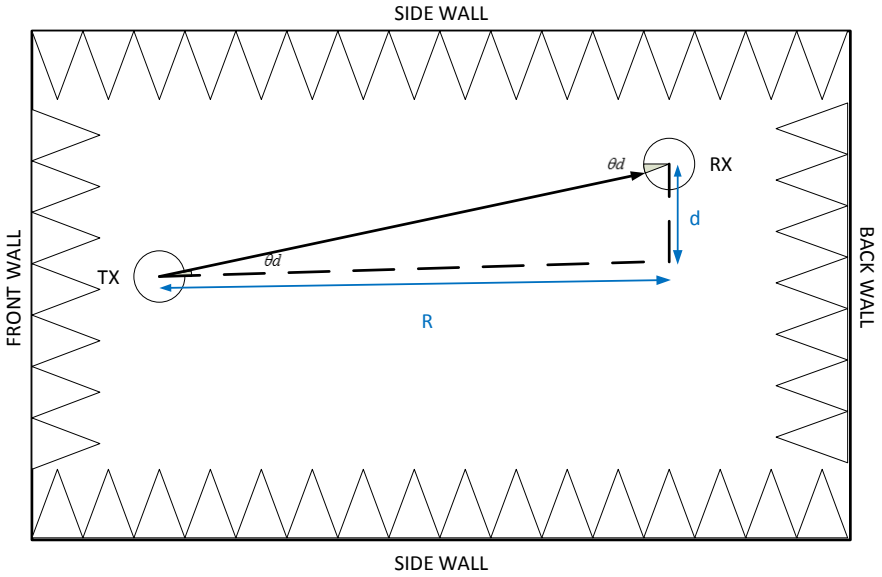

Figure 30 – Transversal scan. Direct ray.

$$\theta d = atan\left(\frac{d}{R}\right) \quad [3\text{-}12]$$

Now, we explained the reflections rays regarding to the side lobes of the antenna pattern. Depending on the receive antenna location these rays will impinge into it or will not. The transmission angle is calculated by applying trigonometry, as in the previous cases. However, computing the receive angle for this scan type is a little bit different. The receive antenna pattern is simplified as a circle, and its equation is calculated. We also calculate the equation of the reflected ray and the system equation is solved. In order to obtain at which height of the circle the ray impinges. Then, with the height and the radius of the antenna, the receive angle is calculated. In Figure 33 an example of this type of reflection ray is shown, with an antenna pattern that has a side lobe at forty five degrees.

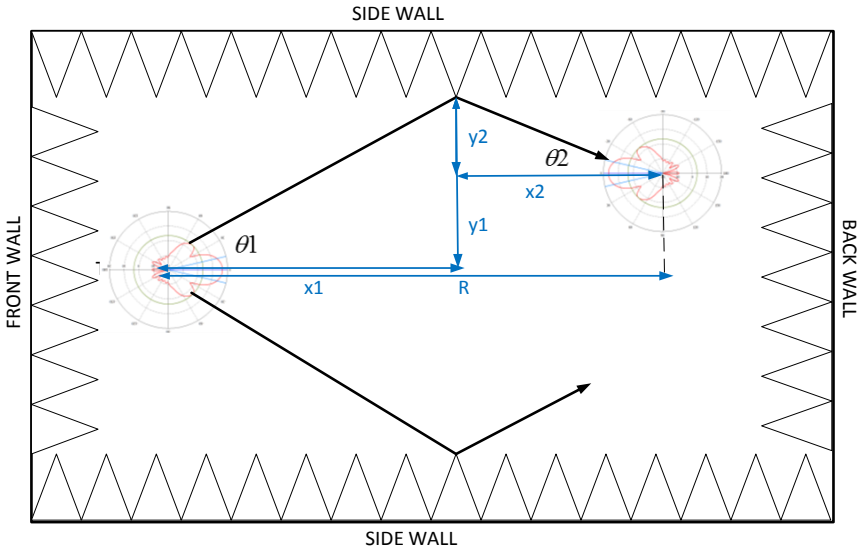

Figure 31 - Transversal scan. Reflections due to the side lobes.

Reflection from the back angle is also calculated when transversal scan is carried out. However, this reflection is not usually as strong as specular ones. See Figure 34.

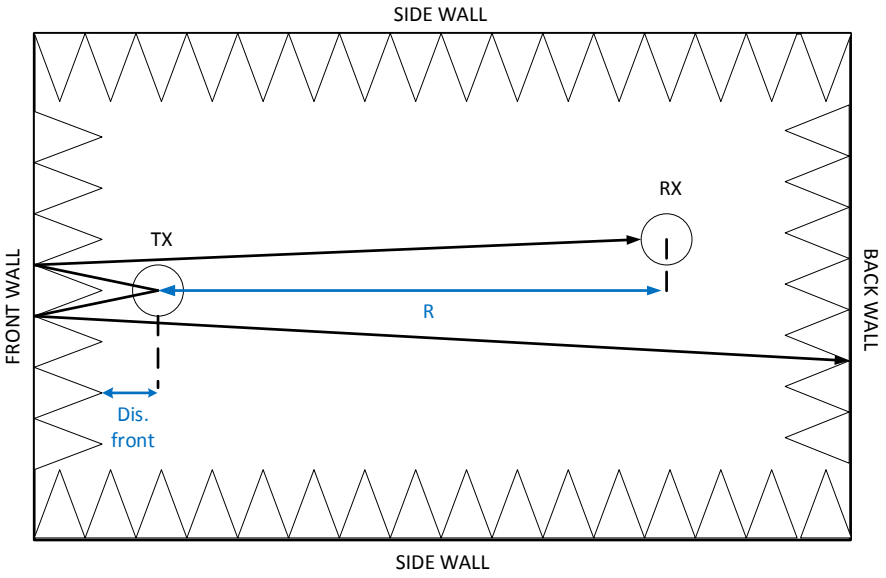

Figure 32 - Transversal scan. Back wall reflections.

When receive antenna is rotated with a certain angle, in order to carry out the scan, the software simulates this turn as well, by adding the turn in the E plane at the incidence angles of each ray. Figure 35.1 and 35.b show an example of the receive antenna at different situations. The first one is when receive antenna is pointing to the transmit, in this case, we see that reflected rays reach 30 and -30 degrees. The second one is when a turn of 90 degrees has been made at the same situation, now the reflected rays impinge at 60 and 120 degrees.

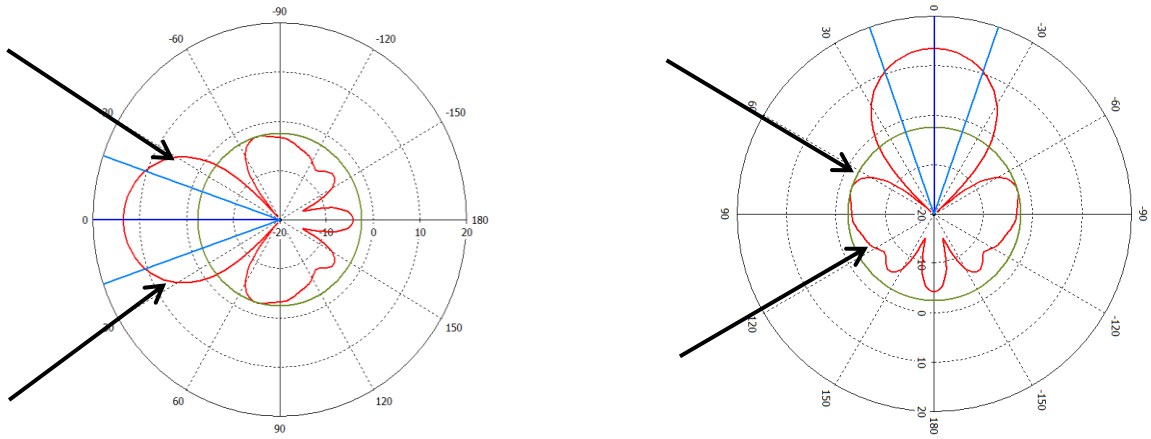

Figure 33 - (35.a) Reflection incidence angle at 0 deg. (35.b) Reflection incidence angle at 90 deg.

- Transversal scan & vertical polarization

In transversal scan, when the polarization is vertical, only specular reflections are taken into account since there are not side lobes in the direction of scan is being made. Here, there is an example of how the reflected ray is calculated in this situation. In this example, the antennas are at the same height from the ceiling and ground, so the contribution of both walls is equal. However, in this software the option of placing the antennas with a certain shift in height, is also supported.

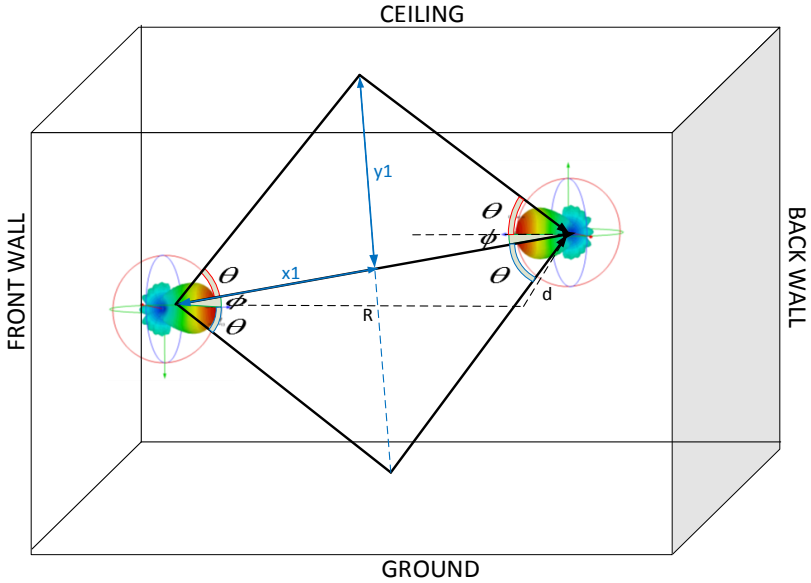

Figure 34 - Transversal scan. Specular reflections due to ceiling and ground.

$$\theta = atan\left(\frac{y1}{x1}\right) \quad [3\text{-}13]$$

$$\phi = atan\left(\frac{d}{R}\right) \quad [3\text{-}14]$$

$$\alpha = 90 - \theta \quad [3\text{-}15]$$

The angles of the reflected ray are calculated with the equation [3-13] and [3-14], where θ is the elevation angle and ϕ, the azimuth. Equation [3-15] computes the incidence angle which the ray reaches to the absorber. As we can see, in contrast to the horizontal case, here the 3D pattern of the antenna is required instead of a plane one. When receive antenna is rotated in azimuth with a certain angle in order to develop the technique, the simulation of this rotation is also required. Figure 37.a shows an example of the reflected rays when receive antenna is pointing to the transmit. In this case, the azimuth of the reflected rays is -30 degrees and elevation 20 and -20, respectively. Figure 37.b shows the same situation when a turn of 90 degrees has been made. In this case, the value of the elevation angle is held constant and the azimuth is 60 degrees.

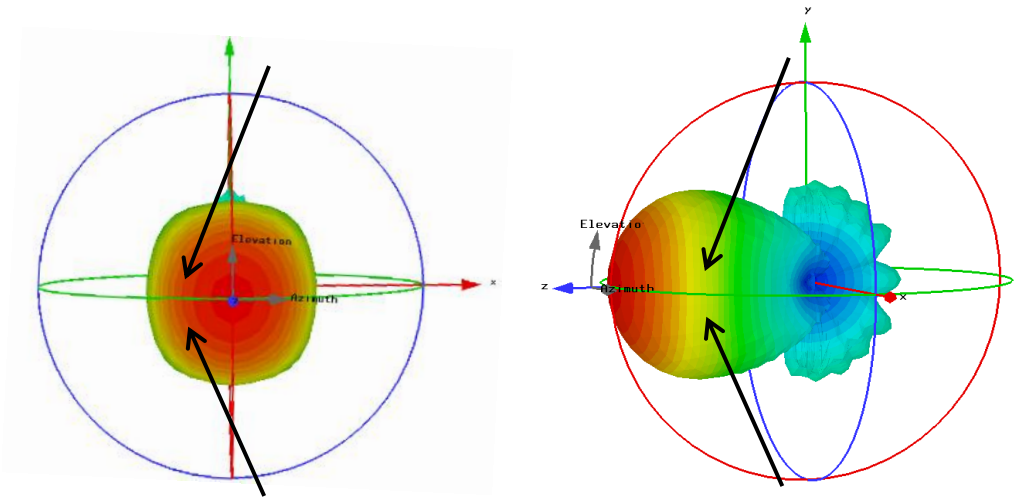

Figure 35 - (37.a) Reflected rays when receive antenna pointing to the transmit.
(37.b) Reflected rays with receive antenna rotated 90 degrees.

- Longitudinal scan & horizontal polarization

In longitudinal scan, there are several types of rays that are taken into account. Reflection rays due to side walls and side lobes are shown in Figure 38. These rays are calculated at different distances between antennas of the longitudinal scan. However, with the difference that now receive antenna is pointed to the back wall. Thus, a shift of 180 in azimuth is introduced. Then if a turn is required, the procedure is the same as in transversal scan at this polarization.

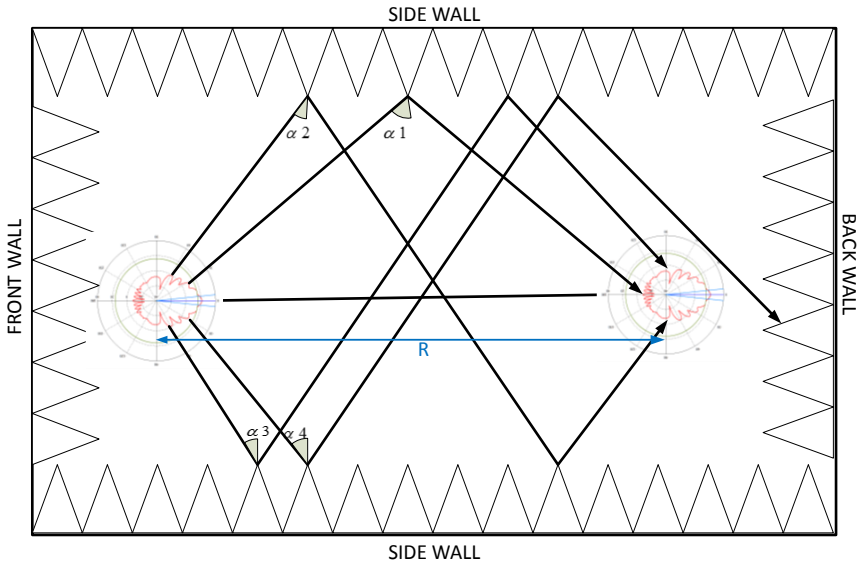

Figure 36 - Side lobe reflections in a longitudinal scan.

The reflections which reach the back wall are also implemented, since the receive antenna is pointed to it. Figure 39 shows and example of these rays, where the side lobe at 45 degrees reaches the receive antenna, when the distance between antennas is R.

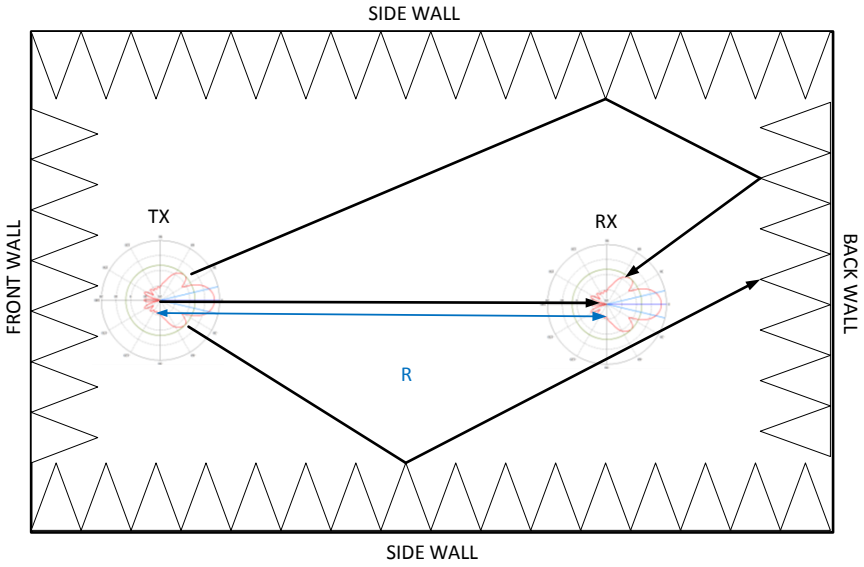

Figure 37 - Side lobe reflections in a longitudinal scan.

- Longitudinal scan & vertical polarization

The implementation of this scan for vertical polarization is exactly the same as in the previous case, but replacing width size by ceiling and ground heights. The only difference is that we are using the 3-D pattern in this case and the rotation procedure is the same as in transversal scan for this polarization

3.2.5 Restrictions

This software was developed under certain conditions that are important to name here.

- The shape of the chamber has to be rectangular.
- All the chamber walls have to be covered by the same absorber type.

There are also more effects in the anechoic chambers that in this software are not considered.

- **Scattering effect**

Even when ray tracing approximation is valid, scattering effect is also produced when reflection rays reach to the absorbers. It is due to impedance mismatches between free space and absorbers. It is mainly produced on the tip of them. There are existing techniques to minimize this effect but it is a costly process [15]. So, it is not usually used.

Factors affecting to the scattering process are the type of material, the shape of the absorber and the non-uniformity of the carbon which the absorber is made of.

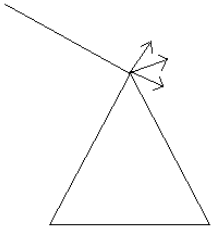

Figure 38 - Scattering effect in a pyramidal absorber.

- **Reflections from the measurement equipment.**

Measurement equipment, such as, positioners, sliding system or metallic plates could introduce reflections in the quiet zone of the chamber.

- **Interferences**

Interference is another possible disturbance factor that we have to keep in mind because the chamber is not shielded.

4 Measurements results and simulations

This chapter is divided into three parts: first section explains some measurements details and results when free-space VSWR technique was developed, the second one explains some simulations results, and the last section is a comparison between measurements and simulations results.

4.1 Measurements results

Two scanning movements were carried out, that is, transversal and longitudinal. The physical distances between antennas and chamber walls when the processes were developed are shown in the Figure 41 and 42, where the unit of the distances are in meters. With regard to the scan dimension, as it was said previously, the quiet zone radius is 0.4 meters. However, it is advisable to record a bigger radius in order to process the obtained measurements correctly. In this case, the scan radius selected was 0.5 meters.

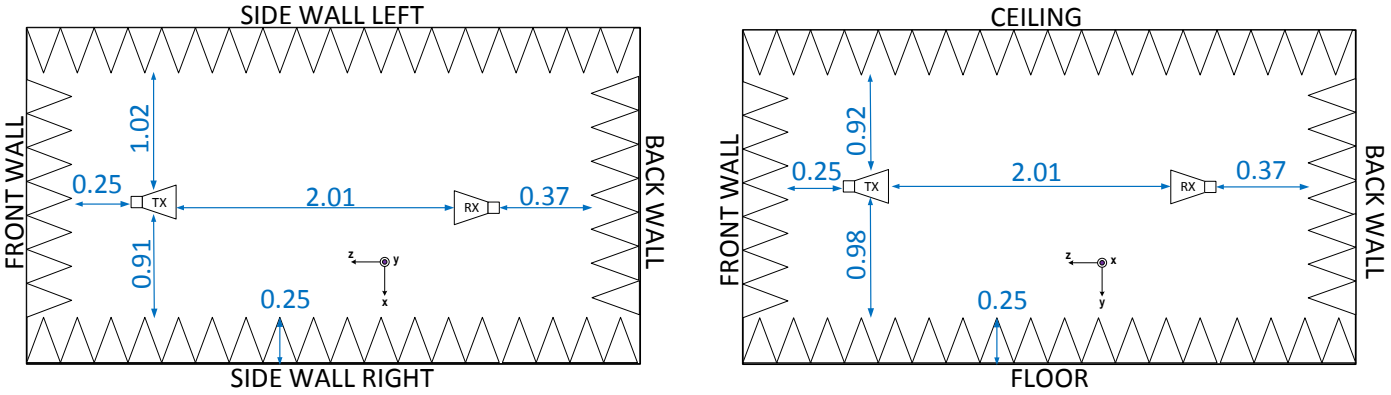

Figure 39 - Chamber situation. Transversal scan.

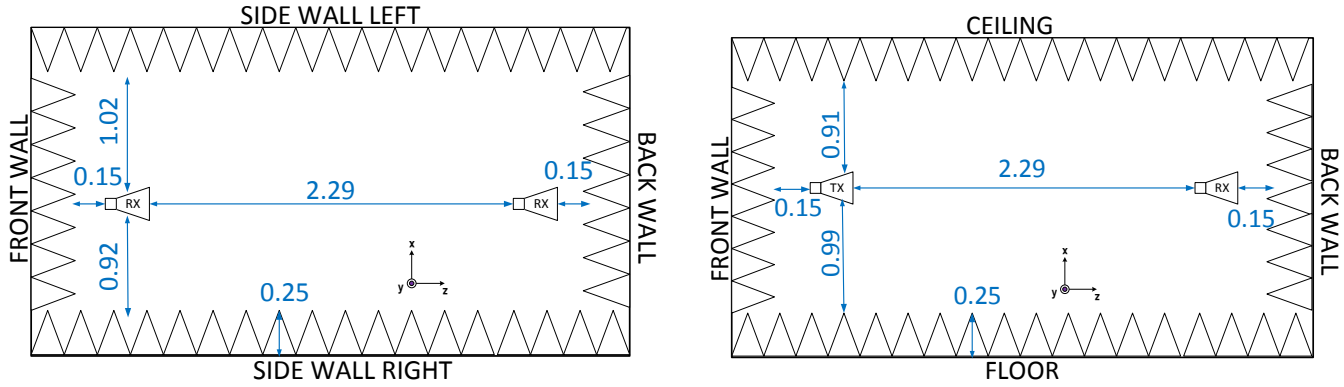

Figure 40 - Chamber situation. Longitudinal scan.

- Alignment

Distances between side walls and ceiling and ground were determined in the alignment process. We can check the errors produced by these misalignments by testing the quiet zone with receive antenna at zero degrees. Differences between measurements at the end of the quiet zone are related to the misalignment error. However, there are also more effects that could affect to these values. Figure 43.a shows the recorded pattern for C horn antenna at zero degrees with horizontal polarization. As we can see in the figure, the level of the measurements at the ends of the quiet zone differs in 0.23 dB. Figure 43.b shows the recorded pattern for vertical polarization, the differences between ends is 0.28 dB. These values are good enough to carry out the procedure.

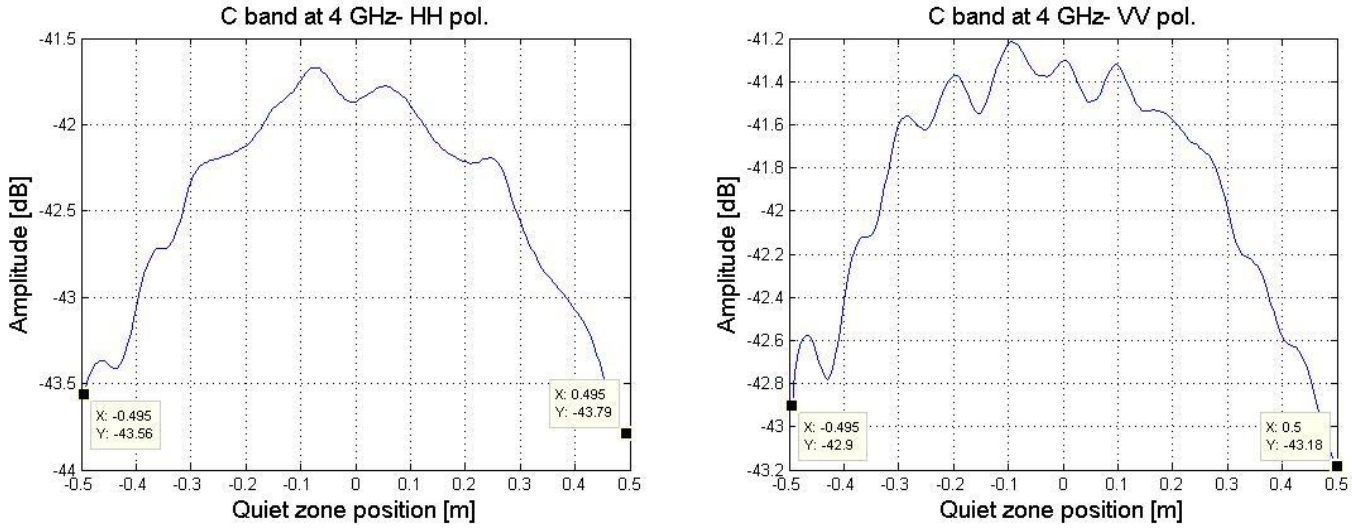

Figure 41 - (43.a) Error due to de misalignment. (43.b) Error due to the tilting.

- Transversal measurements

When the technique scans in the line transversal to the direction of the signal, we record the projection of the antenna patterns. Figure 44.a shows the recorded measurements when the polarization is horizontal at different angular positions. For each situation we computed the ripple and offset value. In this case, the offset value, when the antenna is rotated 15 degrees is 1.39 dB and 4.38 dB when is rotated 30. Ripples inside the quiet zone are 0.275, 0.2945 and 0.4160 dB when the antenna is at 0, 15 and 30 degrees, respectively. As it was said, ripples are produced by chamber walls and measurement equipment, which produces errors in the measurements. Since, at highest frequencies the radiation patterns are more directives, absorbers present more performance and the free space losses are bigger, the recorded ripple are lower. See Figure 44.b.

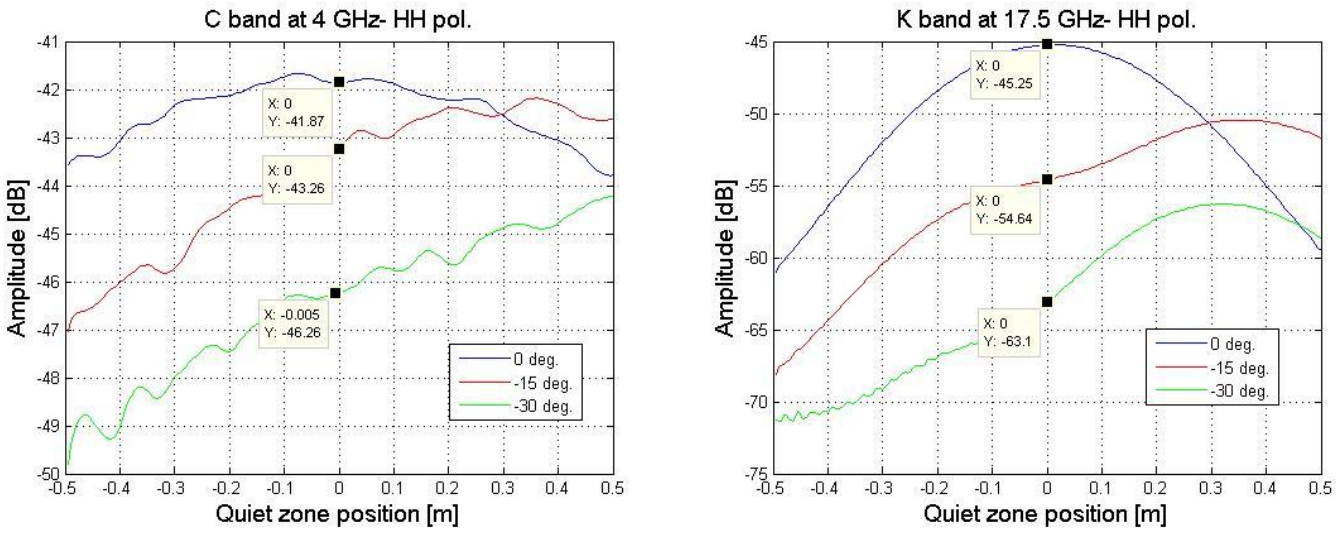

Figure 42 - Transversal scan at different angular positions. (44.a) C band. (44.b)K band. .

Since, the antennas are not situated exactly in the middle of chamber width and height, the obtained ripple values could differ due to this fact. Figure 45 shows measurements of the transversal scan, for horizontal polarization when the receive antenna is rotated 45 degrees to the right and left. As we can see in the picture, a bigger ripple is recorded when receive antenna is rotated minus 45 degrees. At this situation, the antenna is closer to the side wall, so differences between distances could affect to the recorded value. It could also happen that the chamber does not present equal symmetric performance.

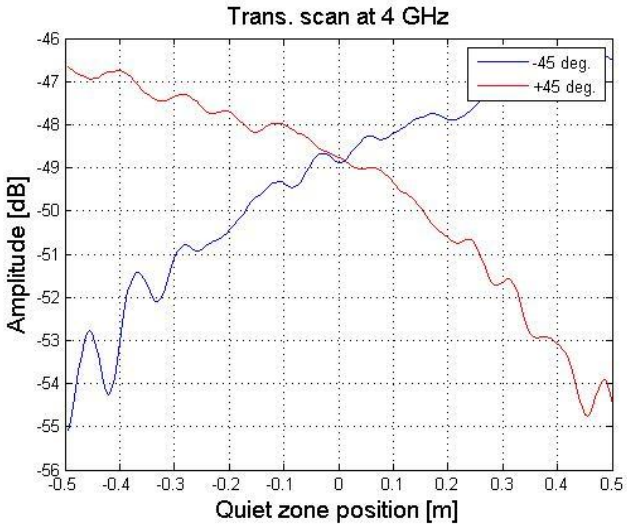

Figure 43 - Transversal scan C horn antenna. Symmetry comparison.

- Longitudinal measurements

Then, results of the longitudinal were analyzed. When this scan is taking place is very important to determine the noise level of the system, since the antenna is pointing to the back wall the recorded levels are low. If these values are below the level of the noise, it means that the device is not able to take this measurement. That is why the dynamic range was measured before starting with this scan.

In order to determine the maximum values of the signal that we will be able to receive during the all process, the receive antenna was pointed to the transmit, and levels were recorded along the quiet zone in the plane parallel to boresight. Figure 46.a shows an example of the recorded levels with a frequency sweep for the K band antenna, when the distance between antennas is maximum in the longitudinal scan. Then, the noise level was measured with the aid of a big absorber which was situated before the receive antenna, in a way that the receive antenna was not receiving signal from the transmit. Figure 46.b shows the recorded noise level and the measurements of the longitudinal scan. As we can see in the picture, the measurements in general are above the noise level, so we can conclude that the recorded values are suitable for this analysis. The dynamic range for this antenna type is 76 dB at the lowest frequency and 70 dB for the maximum.

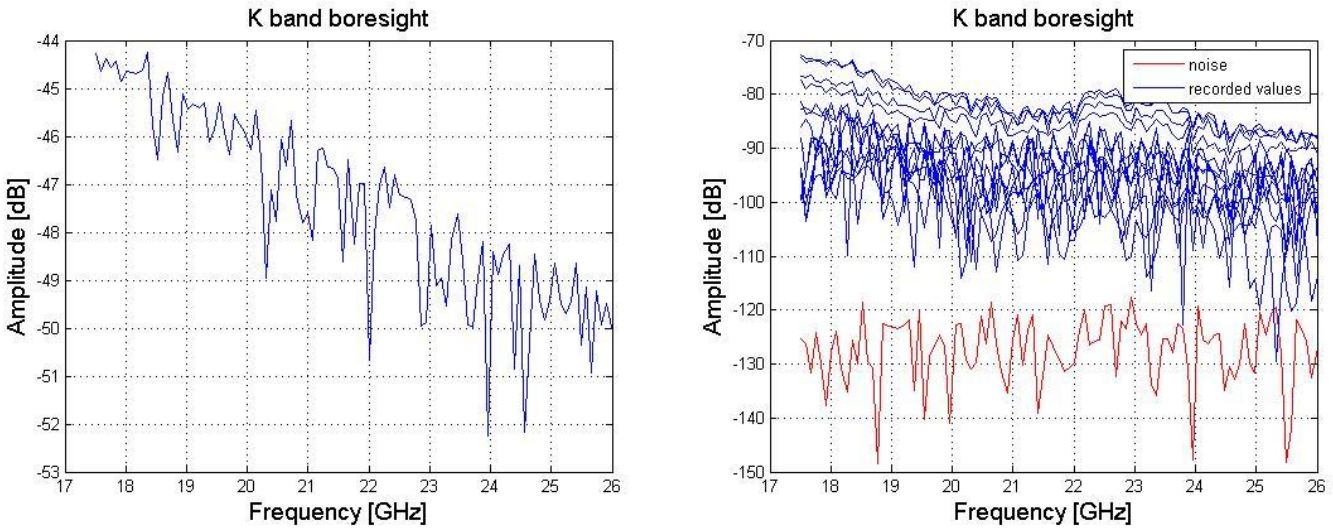

Figure 44 - (46.a) Longitudinal scan at boresight. (46.b) Measurements longitudinal scan and noise level.

In longitudinal scan, the shape of the measurement differs from the transversal scan, where the projection of the pattern is recorded. In this case, we receive with the main beam the reflection from the back wall and the direct ray with back lobe. Figure 47.a and 47.b show the recorded values at different incidence angles from the back wall at 4 and 26 GHz, respectively. If we compare the ripple shapes between figures, as it was expected, changes in the ripples are slower at 4 GHz, due to the phase changes at lower frequencies. With regarding to the amplitude, in both cases, the recorded level is higher when the antenna if rotated 90 degrees. However, this situation could be change if any of the pattern at this angle present a null.

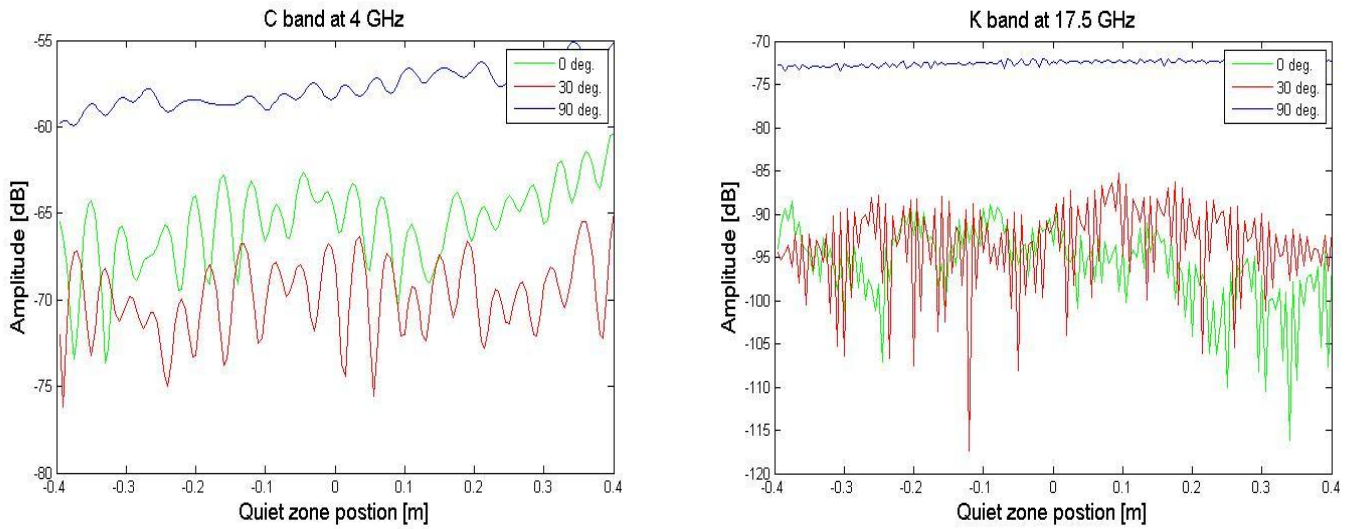

Figure 45 - Longitudinal scan at 0, -30 and -90 degrees. (47.a) 4 GHz. (47.b)17.5 GHz.

- Reflectivity results

As it was said previously, offset and ripples of the measurements are required in order to compute the reflectivity. That is why, a post processing of each measurement was made. Offset values were calculated by fitting the recorded signal. With regarding to the ripples, an envelope of the signal was drawn in order to find the maximum of them. Then, the reflectivity value was computed with equation [2-10]. Below, it is presented the reflectivity results at the first, middle and end frequency of each horn antenna.

	Reflectivity at 4 GHz			
	Trans. Scanning		Long. Scanning	
Angle	Vertical pol.	Horizontal pol.	Vertical pol.	Horizontal pol.
-90	-38,37	-37,61	-38,57	-42,23
-75	-31,75	-34,83	-38,2	-39,06
-60	-32,07	-35,96	-33,17	-37,26
-45	-33,19	-36,7	-36,81	-39,6
-30	-33,07	-35,89	-35,72	-37,99
-15	-36,79	-33,89	-39,82	-36,14
0	-40,93	-35,41	-35,94	-36,37
15	-39,66	-37,48	-35,94	-33,55
30	-35,59	-36,82	-34,4	-37,34
45	-37,06	-38,03	-38,22	-38,74
60	-33,5	-36,62	-35,79	-34,98
75	-36,15	-36,96	-35,27	-39,74
90	-40,01	-37,95	-38,24	-42,44

Table 2 - Reflectivity values at 4 GHz.

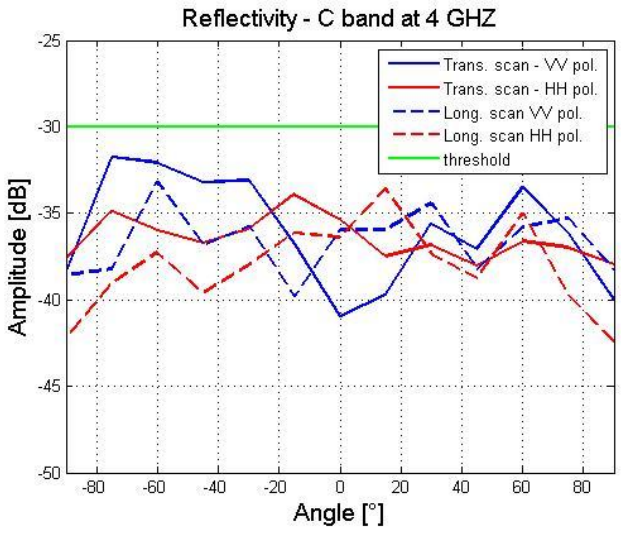

Figure 46 - Reflectivity values at 4 GHz.

	Reflectivity at 5 GHz			
	Trans. Scanning		Long. Scanning	
Angle	Vertical pol.	Horizontal pol.	Vertical pol.	Horizontal pol.
-90	-37,27	-38,9	-38,9	-42,15
-75	-37,98	-35,12	-38,07	-39,47
-60	-35,83	-34,93	-37,72	-38,45
-45	-31,18	-32,12	-35,72	-37,2
-30	-33,85	-36,65	-39,7	-40,46
-15	-38,72	-38,82	-37,24	-37,84
0	-40,3	-34,81	-35,96	-40,91
15	-42,19	-40,32	-39,42	-41,43
30	-38,48	-41,18	-36,74	-37,09
45	-33,46	-40,4	-36,39	-37,06
60	-32,42	-39,84	-37,78	-38,93
75	-33,48	-38,36	-38,31	-38,82
90	-36,95	-39,18	-37,25	-40,59

Table 3 - Reflectivity values at 5 GHz.

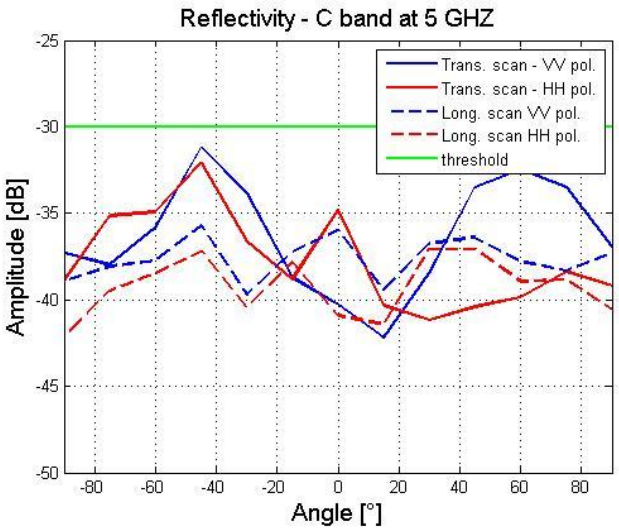

Figure 47- Reflectivity values at 5 GHz.

	Reflectivity at 6 GHz			
	Trans. Scanning		Long. Scanning	
Angle	Vertical pol.	Horizontal pol.	Vertical pol.	Horizontal pol.
-90	-41,48	-40,44	-35,92	-43,96
-75	-35,31	-41,87	-41,03	-40,97
-60	-36,02	-36,67	-37,61	-39,08
-45	-34,51	-43,39	-35,85	-37,61
-30	-36,93	-32,74	-37,95	-38,31
-15	-41,77	-47,17	-39,4	-38,98
0	-48,79	-46,73	-36,99	-39,32
15	-43,92	-40,28	-38,34	-38,03
30	-36,33	-43,27	-39,08	-42,22
45	-36,33	-44,17	-35,94	-35,26
60	-35,69	-38,02	-36,95	-39,34
75	-33,51	-36,66	-38,79	-41,38
90	-40,88	-43,43	-36,93	-45,04

Table 4 - Reflectivity values at 6 GHz.

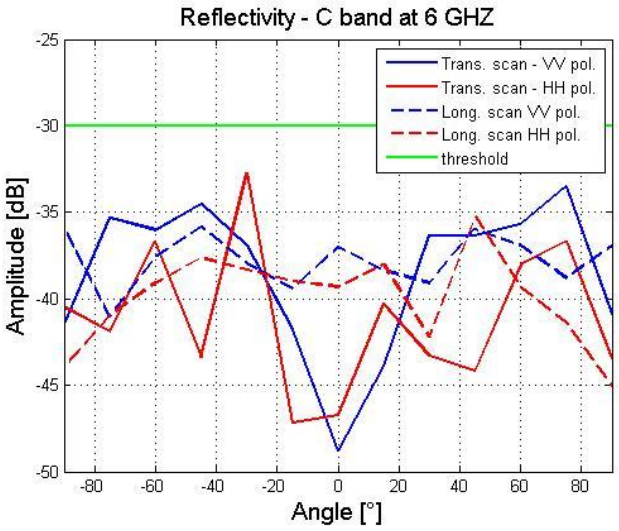

Figure 48- Reflectivity values at 6 GHz.

Table 2, 3 and 4 show the reflectivity values for the C band antenna when both scans are carried out. As we can see here, these values differ for different angles. In order to provide a certain value at each frequency, it was determine a threshold, which ensures that the reflectivity values are below it. As we can see in Figure 48, 49 and 50, the values are similar and lower than -30 dB. Thus, this was the value determined for the C band.

	Reflectivity at 8 GHz			
	Trans. Scanning		Long. Scanning	
Angle	Vertical pol.	Horizontal pol.	Vertical pol.	Horizontal pol.
-90	-43,29	-48,32	-42,78	-47,48
-75	-41,93	-48,35	-42,22	-42,88
-60	-35,3	-48,14	-43,07	-43,23
-45	-36,94	-43,35	-42,74	-42,99
-30	-37,32	-50,85	-42,32	-39,24
-15	-47,09	-55,57	-45,88	-39,95
0	-51,89	-50,81	-46,97	-42,99
15	-46,16	-52,01	-42,37	-41,54
30	-45,62	-48,3	-43,2	-41,6
45	-41,61	-35,3	-43,64	-41,79
60	-36,1	-45,44	-43,58	-40,29
75	-41,54	-47,1	-42,77	-45,37
90	-44,13	-43,05	-42,9	-47,77

Table 5 - Reflectivity value at 8 GHz.

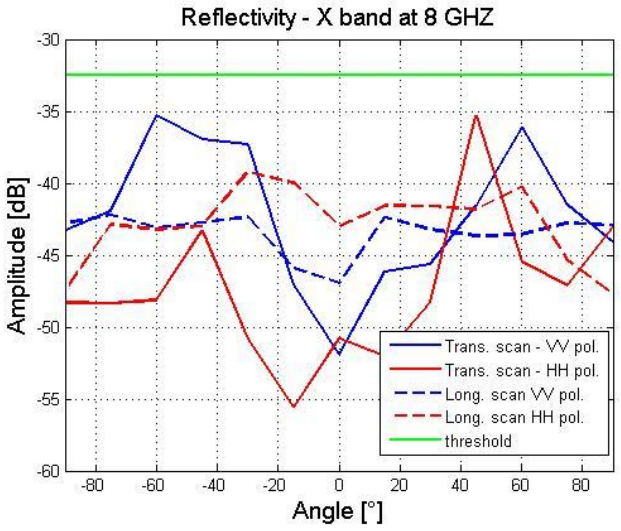

Figure 49 - Reflectivity value at 8 GHz.

	Reflectivity at 10 GHz			
	Trans. Scanning		Long. Scanning	
Angle	Vertical pol.	Horizontal pol.	Vertical pol.	Horizontal pol.
-90	-39,17	-48,21	-43,97	-51,39
-75	-43,7	-51,27	-46,19	-50,17
-60	-42,28	-53,08	-49,45	-46,14
-45	-40,92	-53,7	-49,74	-43,39
-30	-37,88	-47,63	-45,1	-39,47
-15	-44,6	-40,62	-48,13	-43,37
0	-43,96	-46,73	-47,58	-47,9
15	-36,28	-45,41	-46,99	-43,86
30	-41,09	-47,04	-44,88	-39,9
45	-40,87	-48,7	-48,41	-44,27
60	-38,58	-49,08	-48,54	-44,29
75	-36,45	-48,6	-42,52	-45,81
90	-42,09	-51,15	-45,64	-46,82

Table 6 - Reflectivity value at 10 GHz.

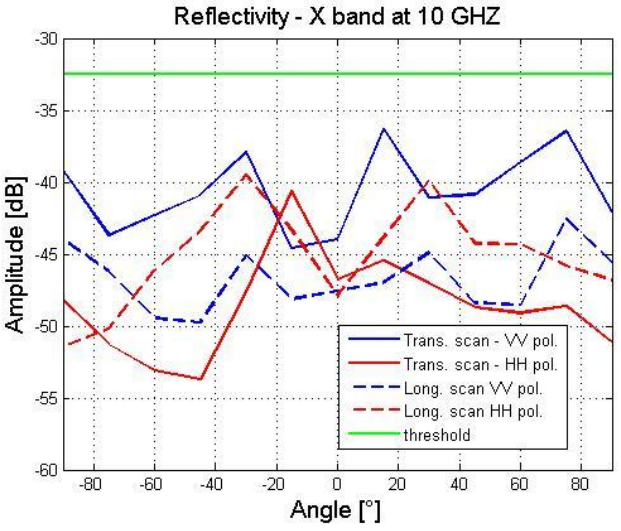

Figure 50 - Reflectivity value at 10 GHz.

	Reflectivity at 11.5GHz			
	Trans. Scanning		Long. Scanning	
Angle	Vertical pol.	Horizontal pol.	Vertical pol.	Horizontal pol.
-90	-51,55	-47,96	-50,64	-56,01
-75	-41,74	-49,73	-49,04	-47,95
-60	-45,26	-53,73	-47,58	-47,91
-45	-48,67	-54,62	-48,57	-44,01
-30	-46,59	-54,47	-49,18	-43,2
-15	-46,67	-57,69	-48,68	-49,68
0	-54,75	-44,79	-49,62	-48,44
15	-51,13	-45	-50,71	-48,39
30	-47,94	-53,45	-48,06	-44,62
45	-46,04	-44,44	-48,54	-43,11
60	-37,72	-47,46	-47,34	-44,31
75	-44,9	-50	-43,13	-43,87
90	-45,07	-48,26	-46,73	-48,94

Table 7 - Reflectivity values at 11.5 GHz.

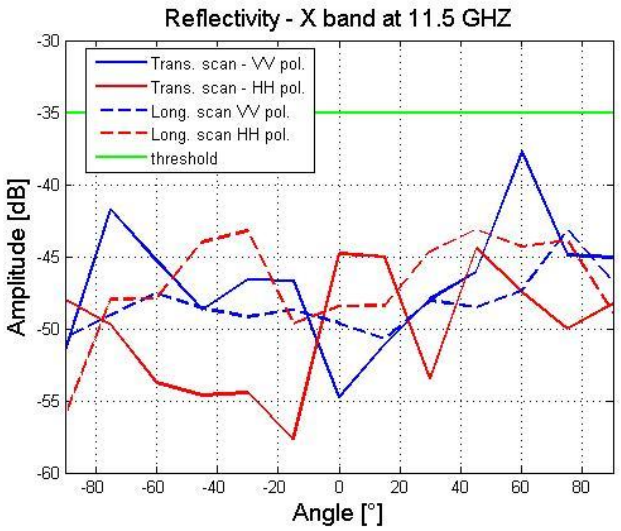

Figure 51- Reflectivity values at 11.5 GHz.

Table 5, 6 and 7 record the reflectivity obtained reflectivity values for the X band. In this case, it is achieved better reflectivity values than C band. This result was expected due to absorbers present better performance at highest frequencies, the antenna pattern is more directive and free space losses are higher. As we can see in the Figures 51, 52 and 53 the reflectivity value for 8 and 10 GHz is -32.5 dB and – 35 dB for 11.5 GHz.

	Reflectivity at 17.5 GHz			
	Trans. Scanning		Long. Scanning	
Angle	Vertical pol.	Horizontal pol.	Vertical pol.	Horizontal pol.
-90	-50,26	-48,1	-53,49	-55,09
-75	-42,64	-44,52	-64,92	-53,2
-60	-46,24	-48,6	-63,24	-52,1
-45	-47,85	-46,27	-58,79	-52,74
-30	-38	-48,42	-50,72	-50
-15	-40,29	-57,33	-53,57	-49,49
0	-	-	-52,33	-49,27
15	-47,57	-50,66	-51,57	-50,31
30	-45	-46,68	-54,86	-47,31
45	-47,17	-37,7	-54,67	-52,94
60	-42,06	-40,31	-58,94	-49,89
75	-42,52	-43,57	-57,54	-51,14
90	-46,24	-42,8	-53,28	-53,42

Table 8 - Reflectivity values at 17.5 GHz.

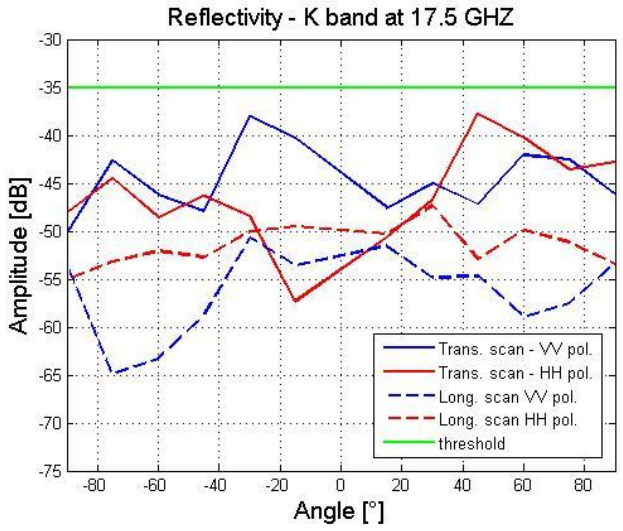

Figure 52 - Reflectivity values at 17.5 GHz.

	Reflectivity at 22 GHz			
	Trans. Scanning		Long. Scanning	
Angle	Vertical pol.	Horizontal pol.	Vertical pol.	Horizontal pol.
-90	-59,42	-51,79	-54,37	-59,42
-75	-48,58	-53,46	-63,54	-57,58
-60	-45,46	-51,24	-70,24	-51,71
-45	-45,86	-53,31	-60,91	-52,71
-30	-52,95	-51,68	-52,8	-53,09
-15	-48,84	-61,39	-49,65	-55,35
0	-	-	-54,9	-54,19
15	-56,41	-53,25	-57,9	-54,19
30	-49,57	-49,36	-54,57	-52,93
45	-48,76	-55,02	-60,77	-50,51
60	-48,03	-45,6	-64,07	-52,24
75	-47,62	-52,98	-59,47	-57,56
90	-53	-50,4	-63,31	-61,4

Table 9 - Reflectivity values at 22 GHz.

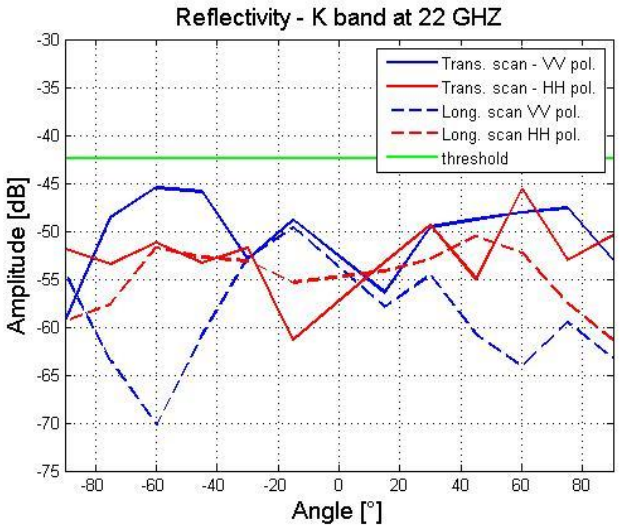

Figure 53 - Reflectivity values at 22 GHz.

	Reflectivity at 26 GHz			
	Trans. Scanning		Long. Scanning	
Angle	Vertical pol.	Horizontal pol.	Vertical pol.	Horizontal pol.
-90	-61,06	-59,95	-59,55	-58,27
-75	-57,34	-59,17	-65,06	-58,43
-60	-60,57	-57,6	-67,36	-53,24
-45	-52,76	-55,61	-61,17	-55,5
-30	-49,27	-56,99	-54,47	-52,51
-15	-56,86	-66.88	-54,6	-59,46
0	-	-	-55,72	-55,79
15	-62,05	-66,04	-53,60	-53,32
30	-49,85	-48,92	-53,72	-51,6
45	-52,99	-48,93	-61,64	-51,89
60	-57,08	-51,26	-63,98	-55,23
75	-55,43	-54,64	-61,63	-55.97
90	-55,74	-53,22	-60,95	-59,17

Table 10 - Reflectivity values at 26 GHz.

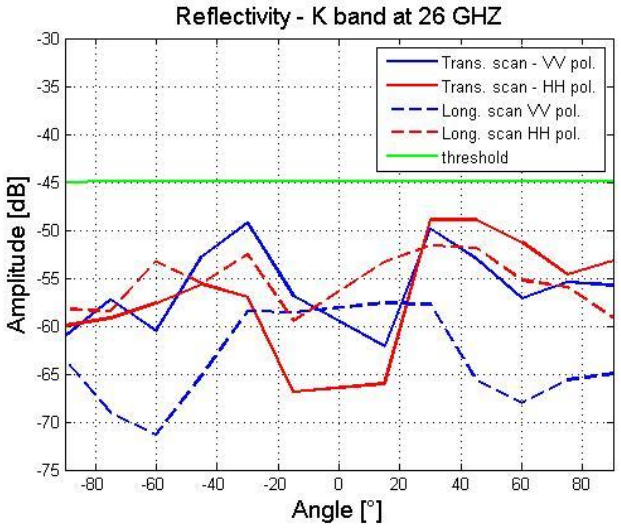

Figure 54- Reflectivity values at 26 GHz.

When free-space VSWR technique was carried out for the K band, the recorded measurements in the transversal scan do not show ripples when the antenna is at 0 degrees. Table 8, 9 and 10 show the recorded values at

17.5, 22 and 26 GHz, respectively. As we can see in the Figures 54, 54 and 56 the threshold for each frequency is -35, -42.5 and -45 dB.

When the reflectivity of the chamber is known, the error associate to the measurements was calculated for the main and the first side lobe by using equation [2-11] and [2-12], respectively. When the main reflections come from two of the walls, we overwrite each equation as in [4-1] and [4-2]. Where Er is computed like in the equation [4-3] and the propagation factor (eq. [4-4]) is the difference of the free space losses between direct and reflected ray. Figure 57 shows the direct and reflected rays when receive antenna is in the middle of the quiet zone. The angle with the reflected ray impinges is forty four degrees. Thus, we can compute the measurement error by replacing the required value at each situation. See Table 11, where the error is computed for the first, middle and last frequency of the operational frequency range. However, the real value of the error could differ, since there are more effects that introduce disturbances in the measurements (Appendix II).

$$error = 1 \pm 2 * \frac{Er}{Ed} * \sqrt{\frac{G(\theta)}{G(0)}} \quad [4\text{-}1]$$

$$error = 1 \pm 2 * \frac{Er}{Ed} * \sqrt{\frac{G(0)}{G(\theta)}} \quad [4\text{-}2]$$

$$Er = Ed * 10^{-\frac{R}{20}} * 10^{-\frac{P}{20}} * 10^{-\frac{G(\theta)}{20}} \quad [4\text{-}3]$$

$$P = 20 * log \frac{Dref}{Ddir} \quad [4\text{-}4]$$

Where,

R: reflectivity
P: propagation factor
Ddir, Dref : distance of the direct and reflected ray, respectively.
G(θ) , G(0) : gain at θ and 0 degrees, respectively.

Frequency (GHz)	P (dB)	G(0°)	G(44°)	G(θ)	R(dB)	Error main beam (dB)	Error SLL (dB)
4	2.83	8.58	4.45	-6.36	-30	**0.044**	**1.27**
10	2.83	15.12	-4.37	-0.35	-32.5	**0.0053**	**0.18**
26	2.83	21.6	2.78	9.03	-45	**0.0019**	**0.034**

Table 11 – Error in the measurements.

As it was expected, we obtain bigger error in the antenna side lobe at each situation. These errors are smaller when the frequency is increasing.

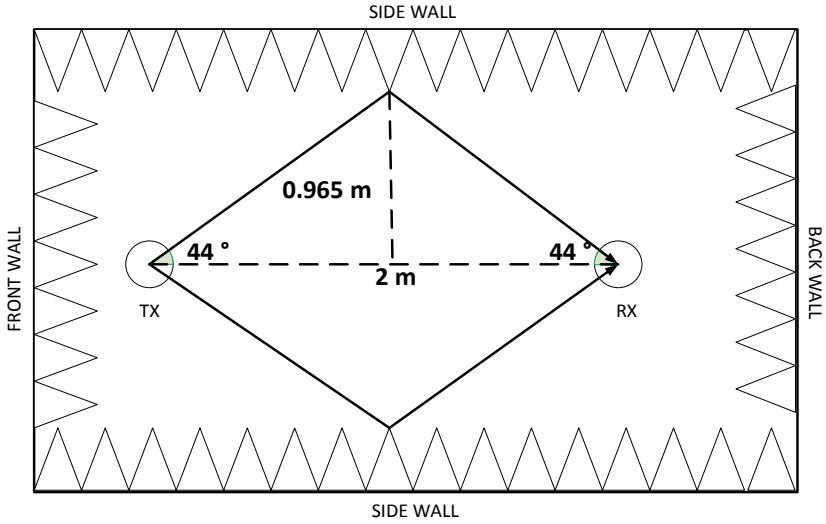

Figure 55 - Chamber view. Error calculation.

4.2 Simulations

In this section, some simulations of this software tool are presented, such as, frequency sweep at boresight and several scans with different input parameters. In order to show the facilities that the software provides. The simulated quiet zone radius is 0.5 meters and the sampling step is 5 mm.

- Frequency sweep

In Figure 58.a and 58.b we can see the results when a frequency sweep is carried out for the C band and X band antennas, respectively. As we know, when the frequency is higher the antenna pattern is more directive, effect that we can appreciate in the figures. However, we have to bear in mind also that the free space losses are bigger at these frequencies, but in this case these differences are smaller than the pattern effect.

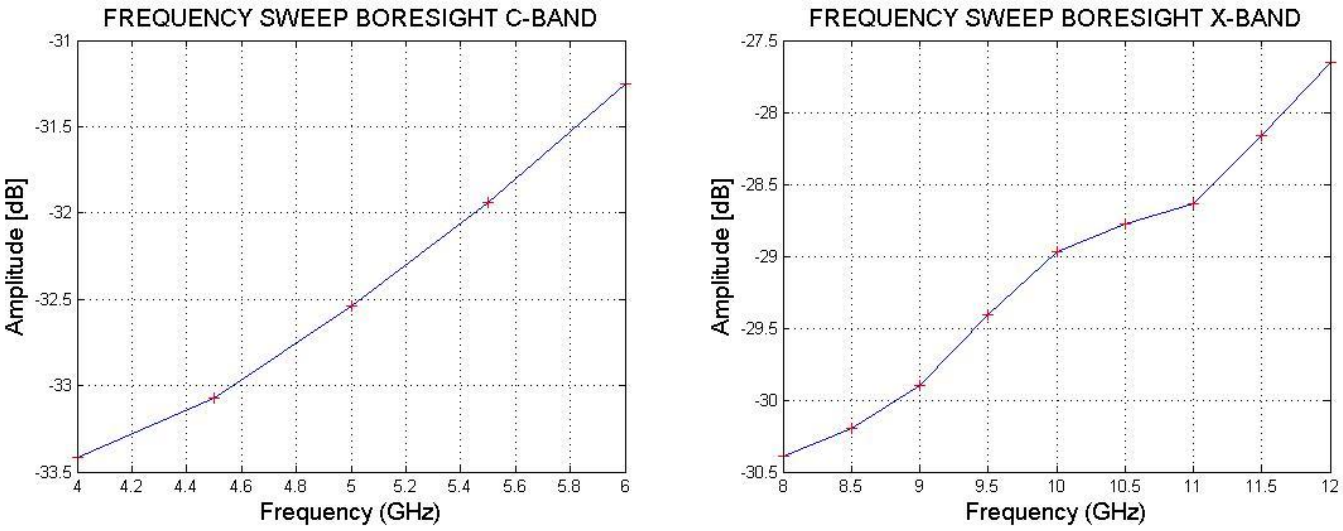

Figure 56 - (58.a) Frequency sweep C band. (58.b) Frequency sweep X band.

- Line scan

Here, simulations of transversal scan, when reflections rays are taking into account are shown. As we can see in Figure 59.a, where the operational frequency selected is 4 GHz, ripples in the measurements are visible. By processing these values and the offset we can compute the reflectivity of the chamber at this situation. In Figure 59.b, the same scan was performed at 26 GHz. In this case, the small ripples that the measurements present is due to pattern resolution. Since, the imported patterns values have a sampling step of 0.25 degrees. However, ripples related to the chamber performance are not visible in the simulations. Figure 60 shows the simulations results when only direct ray is taken into account. As we can see, these small ripples are also visible here. The factors that contribute to the ripples levels change are reflectivity values of the absorbers at these frequencies, the antenna pattern at highest frequency and the free space losses. Thus, the level of the reflections in this case is lower.

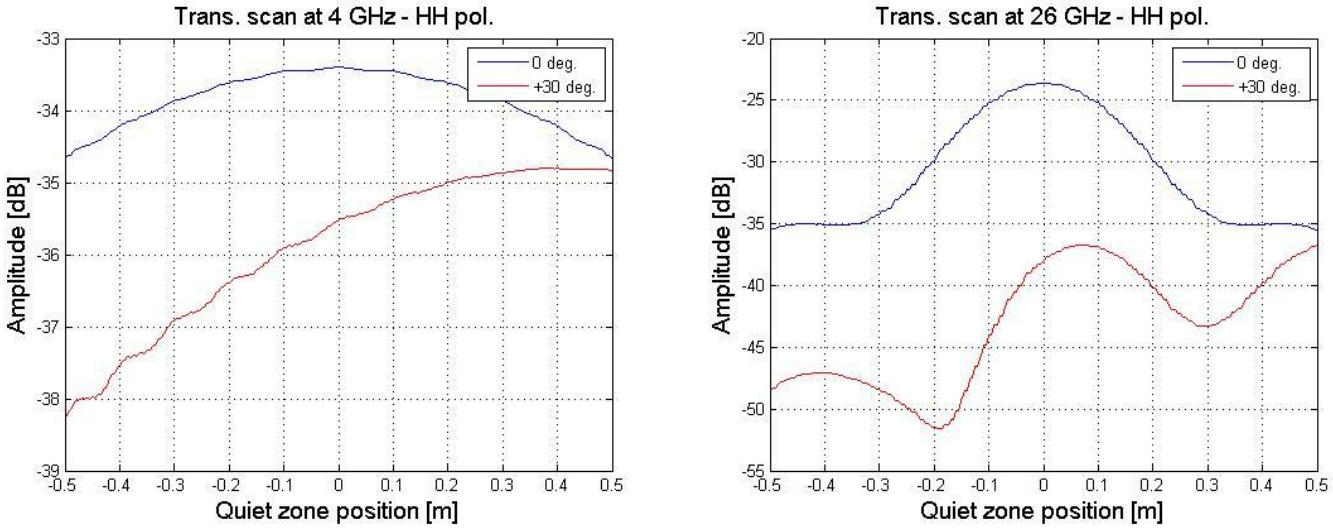

Figure 57 – (59.a) Transversal scan at 4 GHz. (59.b) Transversal scan at 26 GHz.

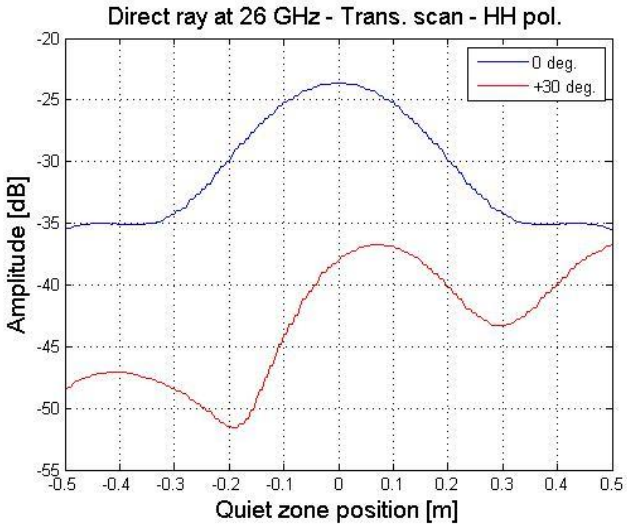

Figure 58 - Transversal scan at 26 GHz. Direct ray.

Reflections at 4 and 26 GHz were simulated in order to check their levels, where the receive antenna is at 0 degrees. See figure 61.

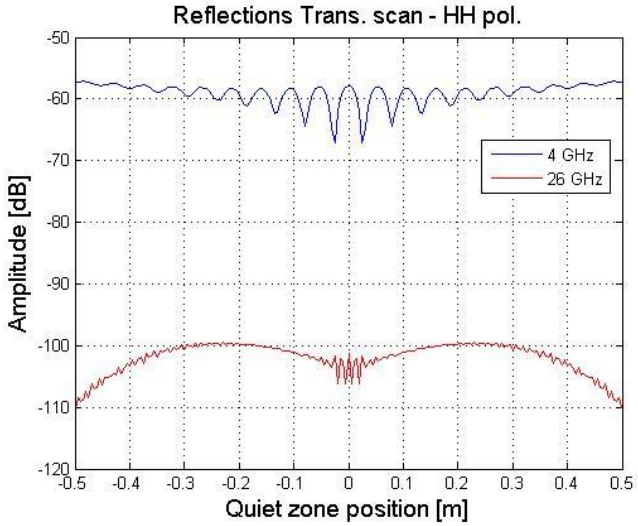

Figure 59 - Transversal scan. Reflection rays.

In this section, it is also shown some of the results of the longitudinal scan. The pattern of the C horn antenna at 4 GHz is represented in Figure 62.a. Figures 62.b, 63.a and 63.b, show the hypothetical recorded values at this frequency when receive antenna is pointing to the back wall and when is rotated 30 and 90 degrees, respectively. As it was expected and taking into account the antenna pattern at this frequency, the level of the direct path is lower when the antenna is rotated 30 degrees, because at this situation is when the direct ray is pointing to the minimum of the pattern. It is also appreciable that in this case, the recorded ripples are bigger.

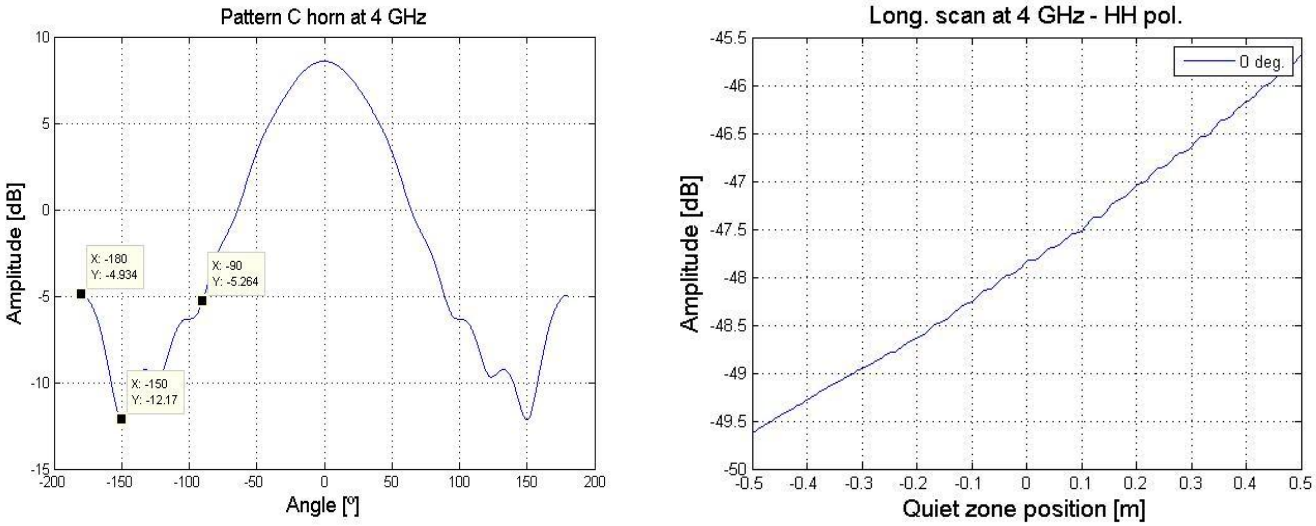

Figure 60 – (62.a) C horn antenna pattern at 4 GHz. (62.b) Longitudinal scan at 4 GHz at 0 degrees.

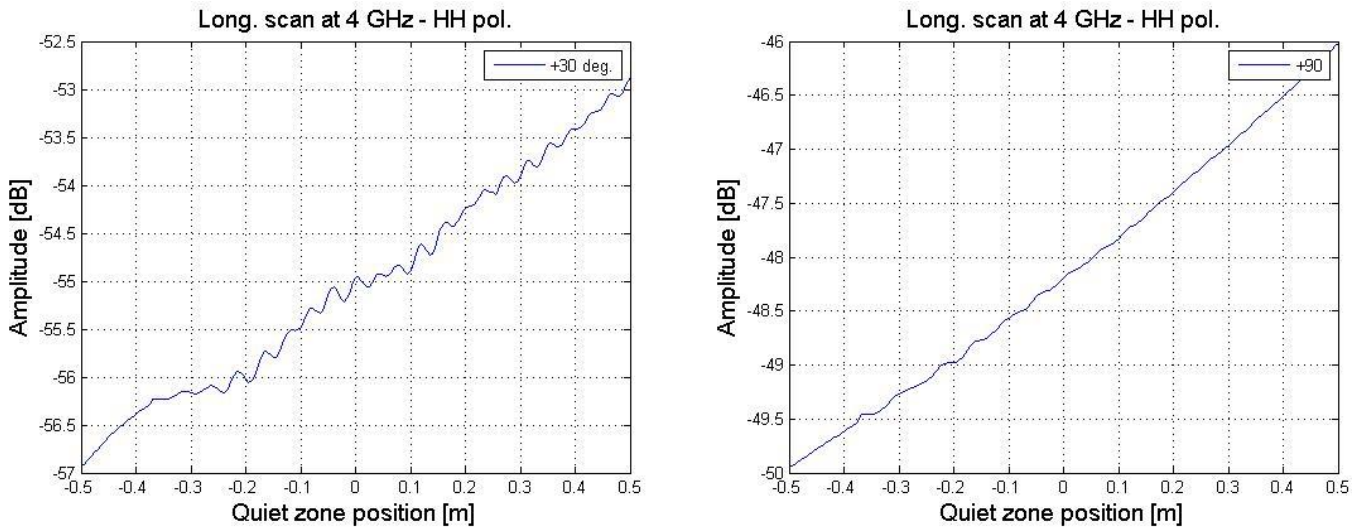

Figure 61 - (63.a) Longitudinal scan at 4 GHz at +30 degrees. (63.b) Longitudinal scan at 4 GHz at +90 degrees.

- Line scan. Step size.

Selecting a suitable step size in the simulation is required. Figures 64.a and 64.b show the results of the transversal scan at 4 GHz with 5 cm and 10 cm scan step, respectively. For this frequency at least it is required a scan step of 7.5 cm ($\lambda/2$). That is way, reflections in Figure 64.b are not visible. Previously, the same scan was simulated with a step size of 5 mm (Figure 59.a), as we can see, in this case the shape of the ripples present more resolution.

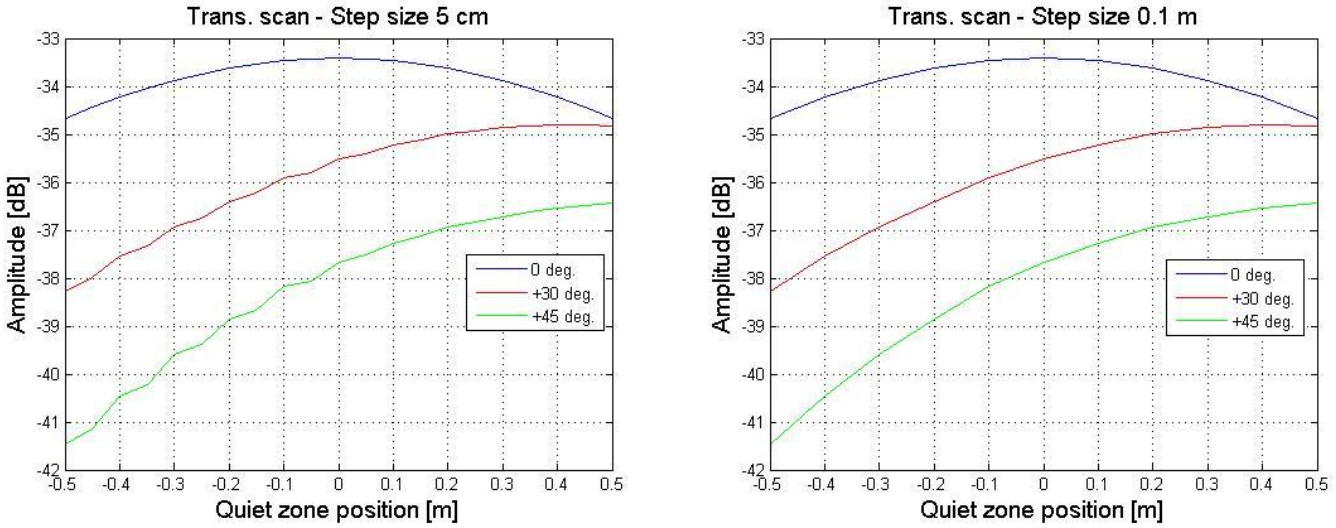

Figure 62 - (64.a) Transversal scan. 5 cm step size. (64.b) Transversal scan. 10 cm step size.

- Line scan. Misalignment and tiling.

In the next figures, we represent the misalignment effect between antennas. Figure 65.a shows the results when transversal scan is carried out and receive antenna is rotated +30 and -30 degrees. At this situation, transmit and receive antenna are aligned and situated equidistant to the chamber side walls. As we can see in the figure, both results are equal, due to the pattern, rotation angle and side wall distance are symmetric. In Figure 65.b a misalignment of 5 degrees when the antenna is rotated 30 degrees is introduced. As we can see, the recorded level of the direct path has decreased due to the transmit antenna is not pointing directly to the receive. Misalignment also produces that the ripples in the measurement are bigger, because the energy that impinges in side wall is also bigger. See Figure 65.b.

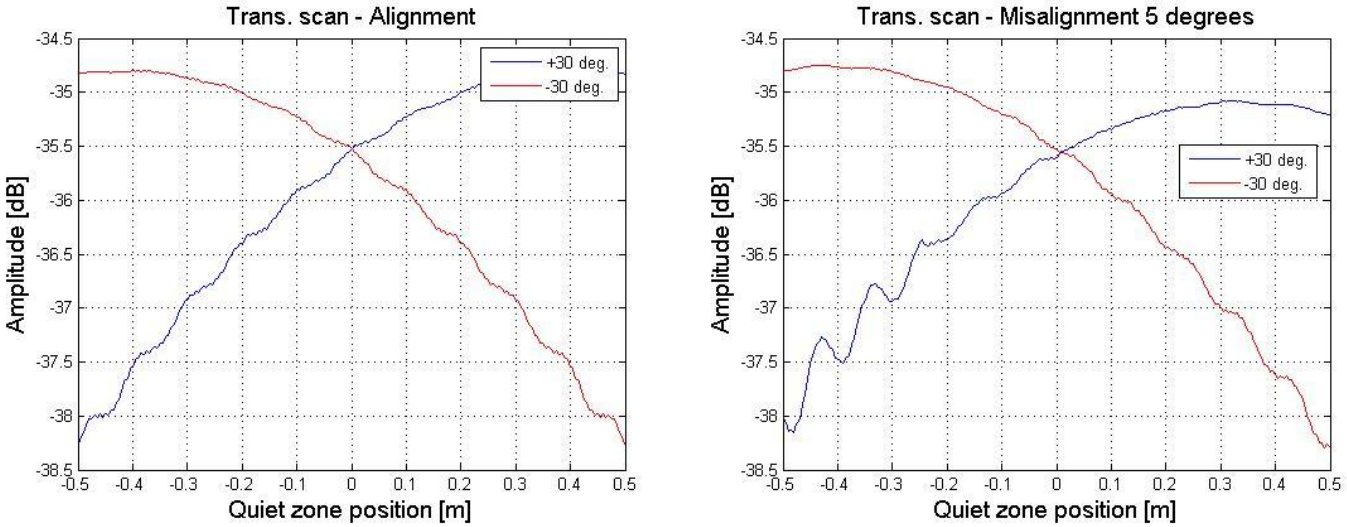

Figure 63 - Transversal scan with a rotation angle of +30 and-30 degrees.
(65.a) Alignment between antennas. (65.b) Misalignment of 5 degrees.

4.3 Comparative between measurements and simulations

In this section, a comparative between the recorded values when free space VSWR technique was run and the results of the software tool when the suitable parameters in the GUI are introduced. See Figure 66. Then, the reflectivity of the simulations were processed and results are compared with the real ones.

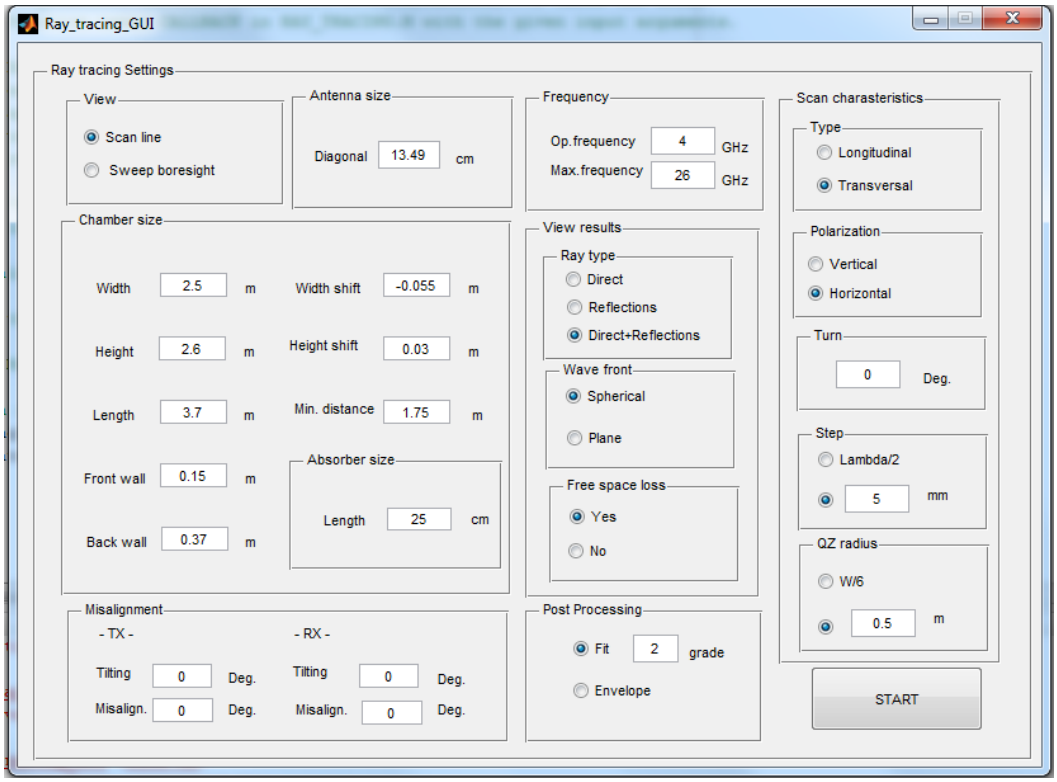

Figure 64 - GUI. Real dimension introduced.

- Transversal scan with horizontal polarization at 4 GHz.

Transversal scan with horizontal polarization measurements are compared. As we can see in Figure 67.a, the shape of the scan at boresight differs from the simulation. The measurement presents asymmetry, this fact could be caused by misalignment, non-centralized positioning of the positioner of the source antenna or due to chamber itself.

In figure 67.b, we can see also differences in the ripples levels. They could be produced by differences in the computed arrival angle and distance of the reflections. Since, depending on how and where the rays impinge into the absorber, the reflectivity and the real distance of the reflection ray differs. However, the main fact that leads to not achieving the same ripple level is that, this tool implements a simple model of the reflections that are produced in the chamber. It does not take into account all the effects that are involved in the real scenario.

Nevertheless, we obtain a good matching in the pattern shape when receive antenna is rotated with a certain angle, as we can see in the Figure 67.b, where the operational frequency is 4 GHz and receive antenna is turned +45 and -45 degrees.

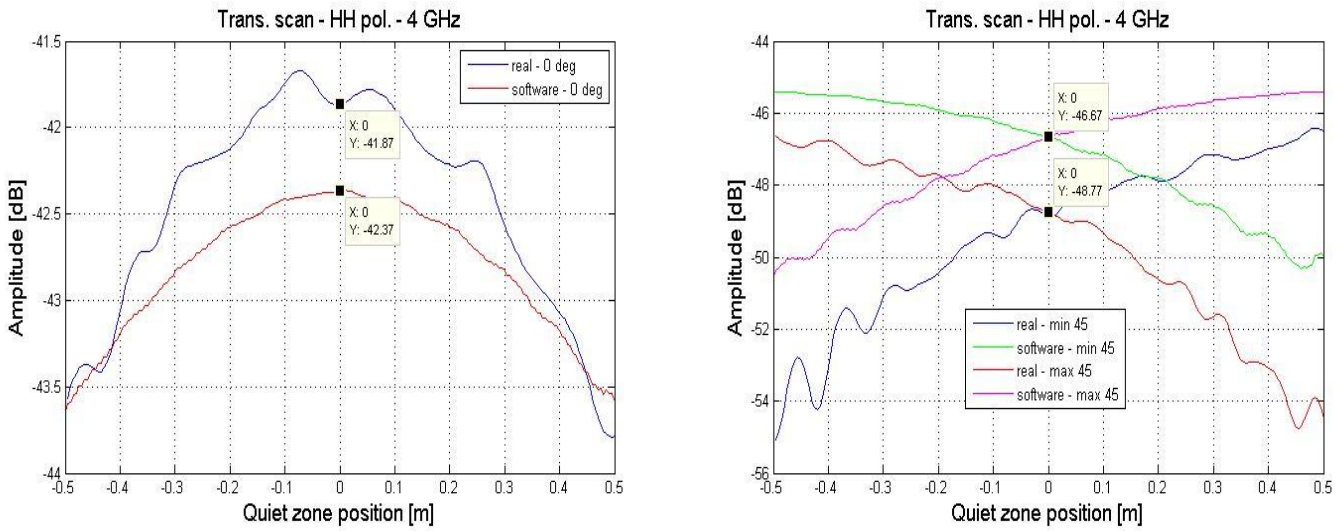

Figure 65 - Real and simulation measurements. Transversal scan. Horizontal polarization at 4 GHz (67.a) At 0 degrees. (67.b) At +45 and -45 degrees.

Ripples in the simulation are visible for the operational frequency range of the C band antenna. However, when we use X band or K band antenna the ripples in the measurements are not visible. Since, the reflectivity values of the absorbers at these frequencies are better and the antenna patterns are more directive. See Figure 68 and 69.

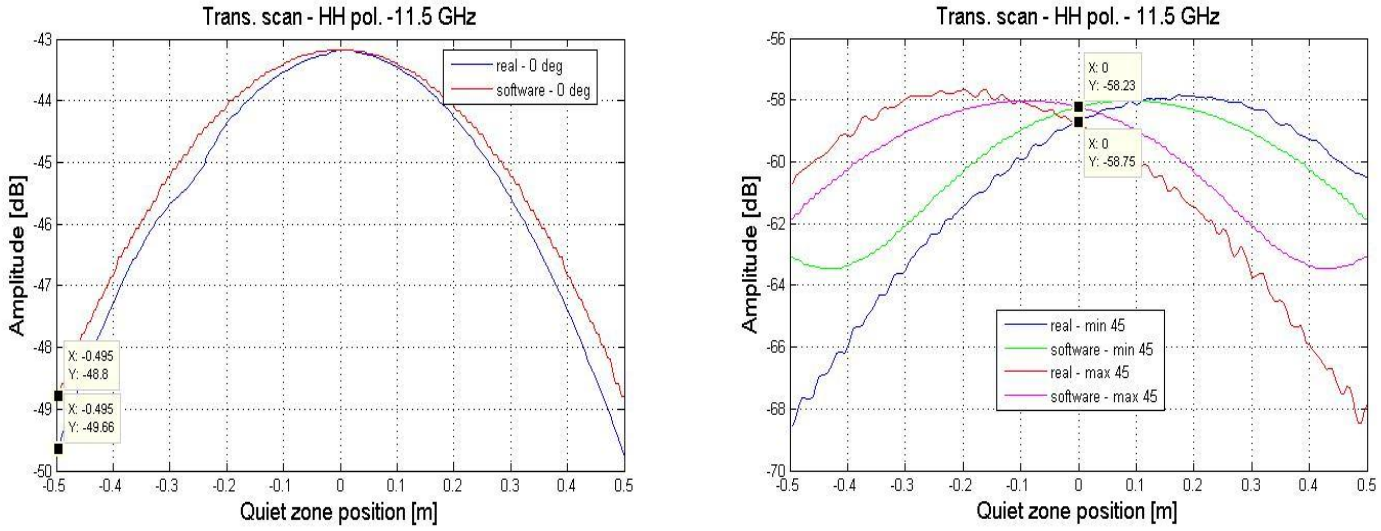

Figure 66 - Real and simulation measurements. Transversal scan. Horizontal polarization at 11.5 GHz (68.a) At 0 degrees. (68.b) At +45 and -45 degrees.

In Figures 68.a and 68.b are shown the results of the measurements and simulations of the transversal scan with horizontal polarization at 11.5 GHz when receive antenna is at 0 degrees and when is rotated 45 degrees in the both senses. As we can see, this tool does not always provide a good approximation of the direct ray. These results are more difficult to achieve when a higher frequency is used, because errors in the

calculation of the distances have more repercussions due to the free space losses. However, the software tool is still matching good at 26 GHz. See Figure 69.

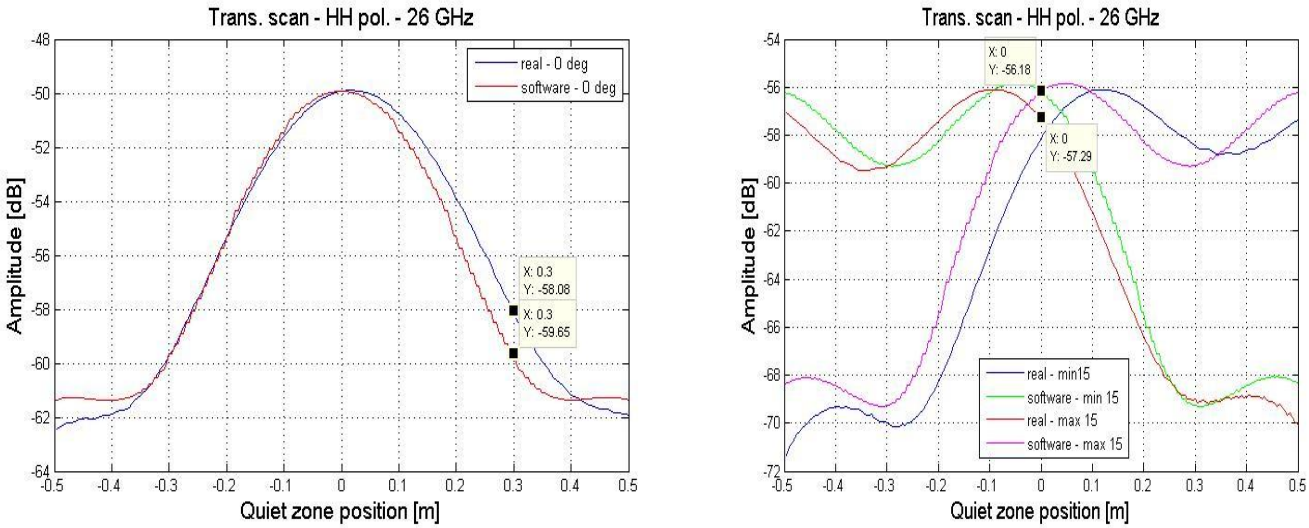

Figure 67 - Real and simulation measurements. Transversal scan. Horizontal polarization at 26 GHz (69.a) At 0 degrees. (69.b) At +45 and -45 degrees.

- Transversal scan with vertical polarization at 4 GHz.

When transversal scan with vertical polarization is carried out, the simulations are not able to reproduce the ripples that the real measurements present. See Figure 70. Since, the antenna pattern at the directions that the software computes the reflection rays do not present side lobes. When receive antenna is in an angular position different from zero, another factor that makes that the level of reflection rays is lower, is that, in this case, we are not pointing with the main beam in the direction that the specular reflections come. See Figure 70.b. Thus, the levels of the reflections, for the vertical polarization case, are lower. However, the shape of the pattern is achieved (Figure 70.a) better than in the horizontal case.

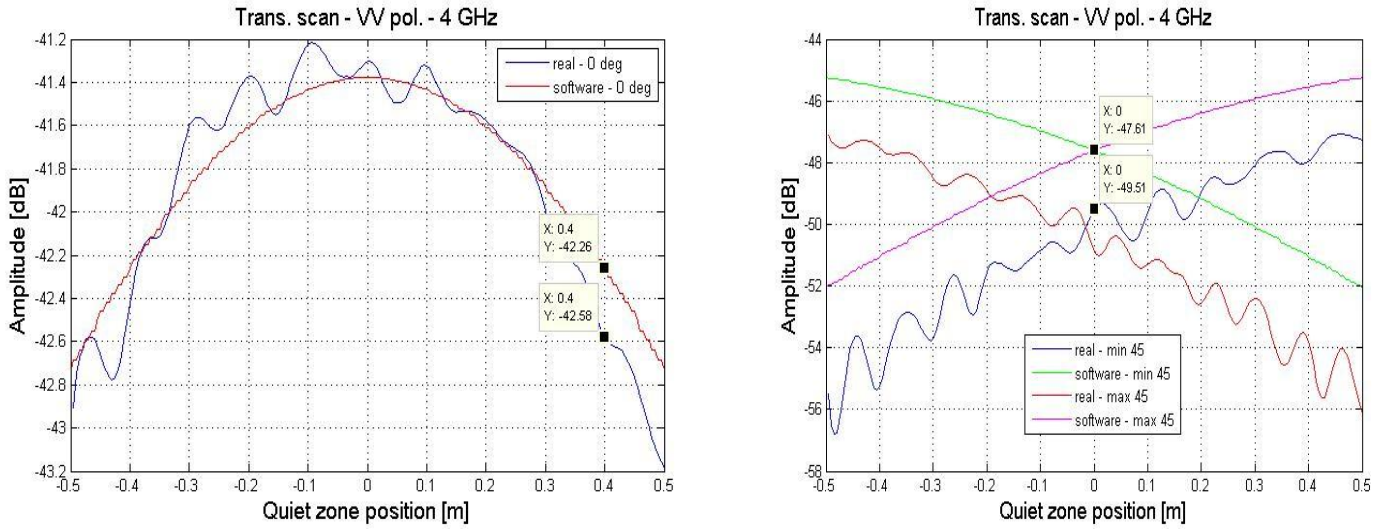

Figure 68 - Real and simulation measurements. Transversal scan. Vertical polarization at 4 GHz (70.a) At 0 degrees. (70.b) At +45 and -45 degrees.

- Longitudinal scan.

In longitudinal scan, simulations and real results are not comparable. Since, the obtained ripples in the simulation are much smaller than the real case. Figure 71.a and figure 71.b show a longitudinal scan with the vertical polarization at 4 GHz when receive antenna is at 0 degrees and 45 degrees rotated, respectively.

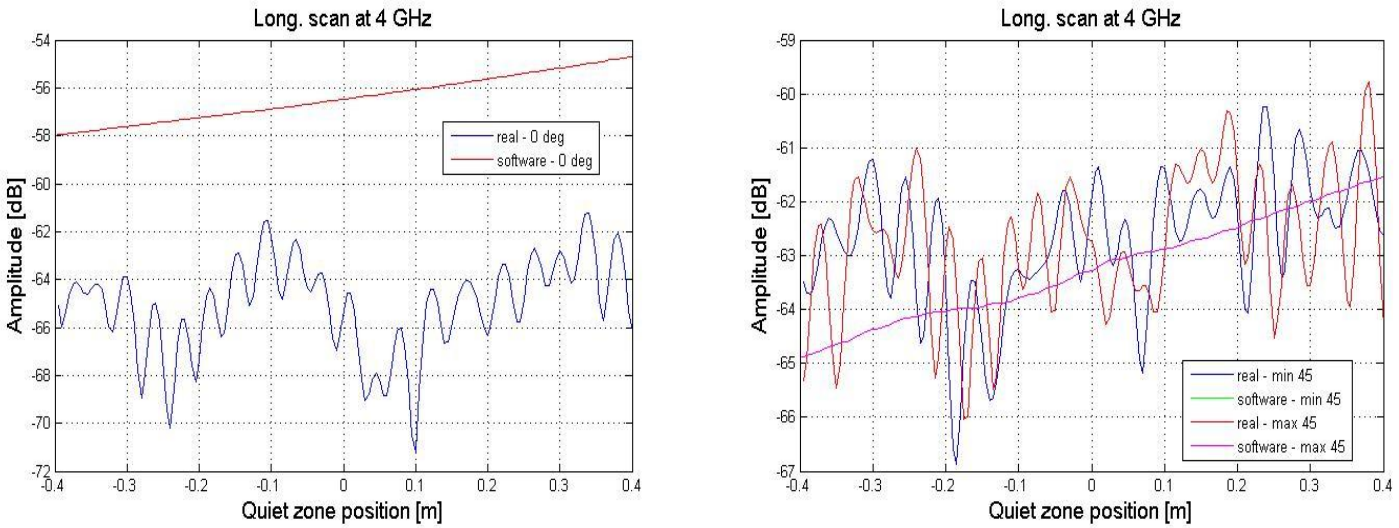

Figure 69 - Real and simulation measurements. Longitudinal scan. Vertical polarization at 4 GHz (71.a) At 0 degrees. (71.b) At +45 and -45 degrees.

We can conclude that at this situation, specular reflections that impinge into the chamber walls and then back wall are not the predominant ones. That is why, it is propose as a future work to enhance the software in order to obtain results closer to the reality.

- Reflectivity of the simulations

As it was said before, the software detects ripples for the C band antenna, when the polarization is horizontal and transversal scan carry out. Figures 72, 73 and 74 show a comparison between the obtained reflectivity values for the real measurements and simulation at 4, 5 and 6 GHz, respectively.

	Reflectivity at 4 GHz		
Angle	Simulation	Real	Error [dB]
-90	-40,01	-37,61	2,38
-75	-33,87	-34,83	0,96
-60	-33,55	-35,96	2,41
-45	-43,81	-36,7	7,11
-30	-46,72	-35,89	10,82
-15	-51,39	-33,89	17,49
0	-55,44	-35,41	20,02
15	-50,98	-37,48	13,49
30	-52,97	-36,82	16,14
45	-52,18	-38,03	14,15
60	-38,39	-36,62	1,77
75	-48,09	-36,96	11,12
90	-42,9	-37,95	4,94

Table 12 – Reflectivity values comparison at 4 GHz.

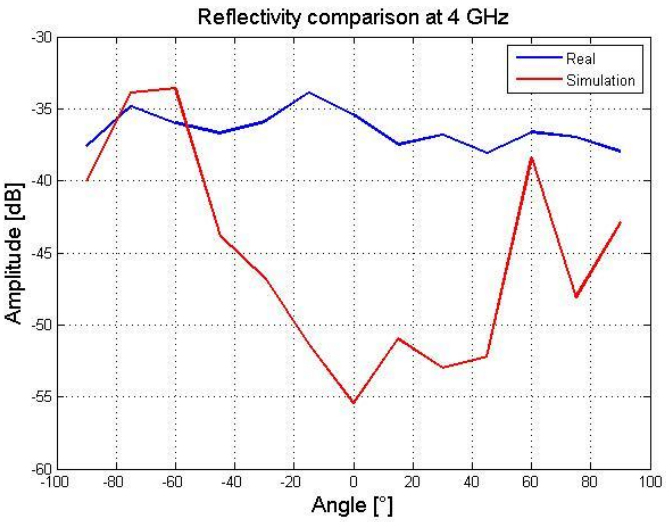

Figure 70 – Reflectivity values comparison at 4 GHz.

	Reflectivity at 5 GHz		
Angle	Simulation	Real	Error [dB]
-90	-47,52	-38,9	8,61
-75	-37,86	-35,12	2,74
-60	-36,33	-34,93	1,39
-45	-38,4	-32,12	6,28
-30	-49,85	-36,65	13,2
-15	-47,86	-38,82	9,03
0	-	-34,81	-
15	-53,12	-40,32	12,79
30	-52,36	-41,18	11,17
45	-45,04	-40,4	4,64
60	-41,88	-39,84	2,03
75	-42,42	-38,36	4,05
90	-55,86	-39,18	16,67

Table 13– Reflectivity values comparison at 5 GHz.

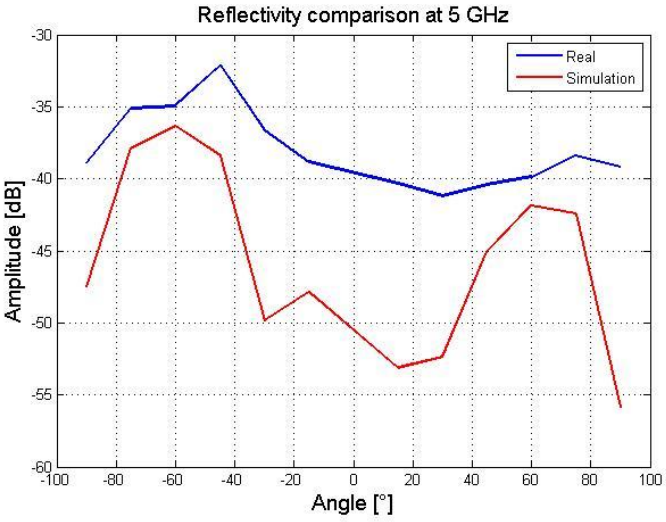

Figure 71– Reflectivity values comparison at 5 GHz.

	Reflectivity at 6 GHz		
Angle	Simulation	Real	Error [dB]
-90	-61,98	-40,44	21,53
-75	-49,36	-41,87	7,48
-60	-38,39	-36,67	1,72
-45	-52,05	-43,39	8,65
-30	-50,21	-32,74	17,46
-15	-56,62	-47,17	9,45
0	-	-46,73	-
15	-59,73	-40,28	19,45
30	-37,53	-43,27	5,74
45	-51,63	-44,17	7,46
60	-41,19	-38,02	3,17
75	-50,34	-36,66	13,67
90	-62,94	-43,43	19,5

Table 14– Reflectivity values comparison at 6 GHz.

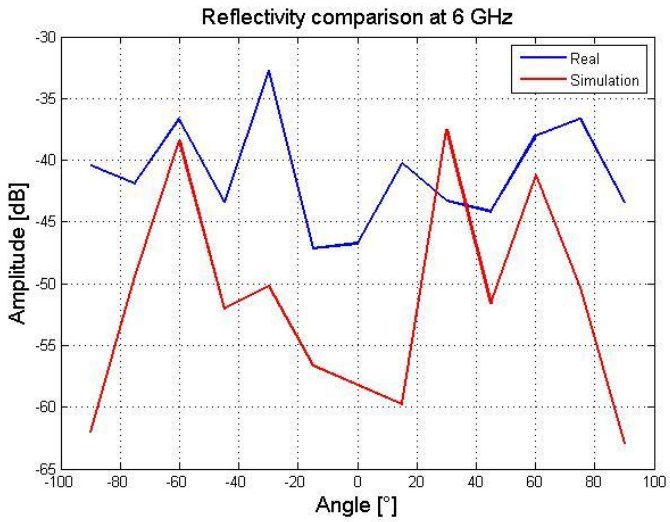

Figure 72– Reflectivity values comparison at 6 GHz.

As we can see in the previous graphs, simulations computes better reflectivity results than the real ones in almost all the cases. That is why, not all the reflections that are taking place in the measurement scenario are considered. However, at the angle that specular reflections are taking place, which is 60 degrees, simulations present smaller errors than 3.17 dB.

5. Conclusions

After characterizing the ATC with the well-known free space VSWR technique, we can conclude that this chamber presents good reflectivity results despite its small size. As it was expected, the chamber provides better reflectivity values when the operational frequency is increasing. Being these values better than -30, -32.5 and -45 dB at 4, 10 and 26 GHz, respectively. The error that the measurement presents, for these frequencies, in the main lobe are 0.044, 0.0053 and 0.0019 dB. As it was expected, the error is smaller when the frequency is increasing. With regarding to the error that it is produced in the side lobe are 1.27, 0.18 and 0.034. However, more error types are involved in the measurement scenario. Thus, the real error value could be much bigger.

Metallic plates, where the antennas are hold, and positioners produce reflections in the chamber quiet zone. In order to avoid disturbances from the plates, absorbers where situated covering them. However, reflections due to the positioners are presented in the measurement scenario. Reflectivity values of MT-25 absorbers where measured in the NRL arch system of the Institute. For the C band case, the obtained measurements are not very reliable, since, it was not possible to resolve the coupling.

The software tool, which implement a first order approximation based on ray tracing, does not work for all the frequencies and scans. The reflectivity values that we get in the simulations are always lower than the real ones. That is why, not all the reflections that are involved in the real measurement scenario are implemented in the software. An enhancement of the software is proposed as a future work.

6. Future work

A possible improvement could be to implement the scattering rays that are presented in the ATC by using the Uniform Theory of Diffraction (UTD) [14], [16]. This phenomenon is relevant when obstacles, in this case, absorbers and measurement equipment have a size that is the same order of magnitude as the wavelength. In this chamber, at the lowest frequency, the absorbers size are comparable with the wavelength. That is why, it is reasonable bear in mind such effect.

Another possible enhancement is take into account the polarization effect. Due to the x-pol component of the transmit antenna and scattering effect, part of the energy impinges into side walls when the polarization is vertical or ceiling and ground in the horizontal case [17]. Hence, specular reflections from the four side walls are considered by multiplying these reflections for a polarization factor [18].

References

[1] Comtest Engineering (2015, April 23) [Online]. Available: http://www.comtest.eu/products/anechoic-chambers/absorbers.html.

[2] L. H. Hemming, "Electromagnetic Anechoic Chambers - A Fundamental Desgin and Specification Guide", *IEEE Press*, John Wiley & Sons, Inc. Piscataway, NJ, 2002.

[3] DMAS (2015, April 23) [Online]. Available: http://dmas.eu/products/.

[4] Cuming Lehman Chambers (2015, April 28) [Online]. Available: http://dl.edatop.com/nsm/mwrf/edatop.com_789_An_Introduction_to_Antenna_Test_Ranges,_Measurements_and.pdf

[5] J. D. X. N. L. L. a. L. X. Z. C. F. Hu, "A low frequency RCS measurement system in an Anechoic Chamber", Electronic Engineering Department, Northwestern Polytechnic University, China, March 2010.

[6] C. L. H. a. E. F. Kuester," Modeling Semi-anechoic Electromagnetic Measurement Chambers", *IEEE Transactions on Electromagnetic Compatibility*, vol. 38, no. 1, February 1996.

[7] H.Shakhtour, J. Pamp, D. Heberling, H. de Groot , B. de Groot, "Quiet Zone Characterization of a Built-It-Yourself Antenna Test Chamber", Institute of High Frequency Technology, RWTH Aachen University, EUCAP 2015.

[8] G. Cottard, Y. Arien, "Recent Microwave Absorber Wall-Reflectivity Measurement Methods", *IEEE Antennas and Propagation Magazine, Vol. 50, No. 2, April 2008*.

[9] J. Appel-Hansen, "Reflectivity Level of Radio Anechoic Chamber", *Antennas and Propagation*, *IEEE Transactions on, vol. 21, no. 4, pp. 490,498, July 1973.*

[10] D. Segovia, "Antennas Measurements, Laboratory of Radiofrequency", Radiofrequency group, UC3M Carlos III de Madrid, Feb. 2013.

[11] D. Segovia, "Measurements exercises, Laboratory of Radiofrequency", Radiofrequency group, UC3M Carlos III de Madrid, Feb. 2013.

[12] P. Joseph (2015, April 23) [Online]. Available: http://www.antenna-theory.com/ tutorial/ electromagnetics/ electric-field-boundary-conditions.php.

[13] D. B. C. C. B. Williams, "Transmission Electron Microscopy", *A Textbook for Materials Science, Second Edition,* 2009, Chapter 2.

[14] R. G. K. a. P. H. Pathak, "A uniform geometrical theory of diffraction for an edge in a perfectly conducting surface" Proceedings of the IEEE, vol. 62, no. 11, November 1974.

[15] Stephen A.Brumley, "Evaluation of microwave anechoic chamber", DTIC, Arizona State University, May 1988.

[16] A. Tzoulis, T. Vaupel, T. Eiber, "Ray Optical Electromagnetic Far-Field Scattering Computations Using a Planar Near-Field Scanning Techniques", *IEEE transactions on Antennas and Propagation*, Vol. 56, no. 2, Feb. 2008.

[17] A. Alayron, A. Molisch, F. Tufvesson, “Fading Characterization in Semi-Anechoic Chamber with Artificial Scatters for Mean Effective Gain Measurements of Wireless Handheld Terminals”, Mitsubishi Electric Research Laboratories, TR2008-043, Aug. 2008.

[18] Birkbech College (2015, April 27) [Online]. Available: http://pd.chem.ucl.ac.uk/pdnn/diff2/polar.htm

[19] Rohde Schwarz (2015, April 23) [Online]. Available: http://es.slideshare.net/RohdeSchwarzNA/signal-integrity-testing-with-a-vector-network-analyzer-30667374?qid=ce06bfe8-7ffb-423a-87d9-6e53f4259d46&v=qf1&b=&from_search=6.

[20] M. W. L. N. K. P. a. M. B. R. Przesmycki, "Antenna Gain Measurement by Comparative Method Using an Anechoic Chamber", *PIERS Proceedings, Moscow, Russia, Augus*t 19–23, 2012.

[21] M. Stecher, "Uncertainty in RF emissions measurements". Revision of CISPR 16-4-2.

[22] C. A. Balanis, "Antenna Theory Analysis and Design", John Wiley & Sons, Inc. Second Edition.

List of figures

Appendix

Appendix I: Calculation specular reflections in the transversal scanning

In order to compute the specular reflection rays when the transversal scan is carried out similarity of triangles is applied [A-1].

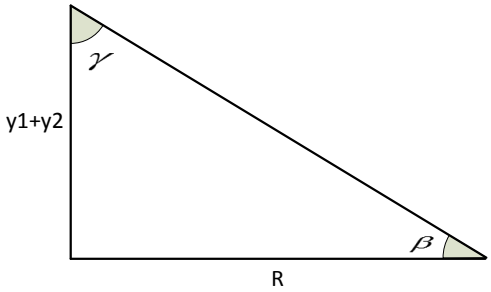

Figure 73 - Similar triangle of specular ray

$$tg\beta = \frac{y1+y2}{R} \qquad \text{[A-1]}$$

Equation [A-2] computes the distance that the reflected ray impinges into the absorber and equation [A-3] the distance from the absorber to the receive antenna.

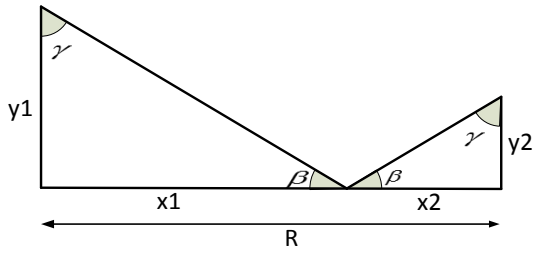

Figure 74 - Reflection ray geometry

$$x1 = \frac{y1}{tg\beta} = \frac{y1}{y1+y2} * R \qquad \text{[A-2]}$$

$$x2 = \frac{y2}{tg\beta} = \frac{y2}{y1+y2} * R \qquad \text{[A-3]}$$

Appendix II: Error and uncertainty in the measurements.

The error type in the measurements can be difference into three groups, which are drift, random and systematic errors. In these appendix an explanation of these error types is given, as well as, discussion about uncertainty in the measurements.

Systematic errors are caused by the non-ideal components in the VNA and test setup. By calibration we can remove this error type, because they are repeatable [19].

Drift errors are caused by changes in the environment after the calibration. Such as, temperature or humidity in the measurement environment. We can determine the best temperature and humidity conditions taking the measurements at different situations, and then, evaluate the obtained error. Normal temperature conditions inside an anechoic chamber, are around 20°C-25°C and humidity of 30%-85% [20]. In some chambers, there are controllers to maintain the chambers below certain conditions. This is a way to minimize this error type.

Random errors are caused mainly by the instrument noise. This error type cannot be remove only minimized. The way to minimize them is by using high quality equipment and good measurement practices. However, in consequence the price will be higher, so depending the application and the required error, we can select a suitable equipment.

Uncertainty of the measurement is a relevant parameter mainly due to the drift and random errors. That is means that we can obtain different measurements values below the same input conditions. There are several type of uncertainty. Below, it is explained some of them [21].

- Standard uncertainty

It is the standard deviation of the measurement (*us*), which is the mean of the error of *n* independent measurements that they have been taken under the same conditions. Depending on the type of distribution, the way to compute the error, changes. For normal distribution the uncertainty is computed as:

$$\overline{us} = s(q) = \frac{s(qj)}{\sqrt{n}} \qquad \text{[A-3]}$$

Where,

$$s(qj) = \sqrt{\frac{1}{n-1}\sum_{j=1}^{n}(qj - \overline{q})^2} \qquad \text{[A-4]}$$

n: number of measurements

qj: measure j of the magnitude

$\overline{q}$: mean value of the magnitude with n samples

Other typical distributions are Lognormal, rectangular, triangular u-shaped, trapezoidal. For measurements which have been taken with logarithm base, it is used Lognormal distribution.

- Combined standard uncertainty

Every measurement has got different types of errors, which are statistically independent. Hence, the way to calculate the resultant uncertainty is expressed in the equation [A-5]. It is known as *The Law of Propagation of Uncertainty*. Where the errors, due to different focus, are multiplied by sensitivity coefficient.

$$uc = \sqrt{c1^2u1^2 + c2^2u2^2 + \cdots + cn^2un^2} \qquad \text{[A-5]}$$

u1, u2, …, un: error in the measurement
c1, c2, …, cn: sensitivity coefficient of the measurement.

- Expanded Uncertainty

It is the range of error values which are measured with a certain probability. Depending on the probability of the error, a coverage tabulated factor is used. The idea is to be aware if the error of the measurement is below certain limits. When the combined or standard uncertainty is calculated, and we know the probability associated to this error, the coverage factor is applied to the error. The result is checked if it is below certain limits.

$$ulab = k * uc \qquad \text{[A-5]}$$

Where,

k: coverage factor
uc: combined or standard uncertainty measure

If $u_{lab} \leq u_{cispr}$, the error do not exceed the margin.
If $u_{lab} \geq u_{cispr}$, the error is bigger and we have to analyze what is going on in this measure.